Universidade de Aveiro Departamento de Física,
2013

Anselmo Marques

Supercondutores de múltiplas bandas frustrados

Frustrated Multiband Superconductors

Universidade de Aveiro Departamento de Física,
2013

Anselmo Marques

Supercondutores de múltiplas bandas frustrados

Frustrated Multiband Superconductors

"The behaviour of large and complex aggregates of elementary particles, it turns out, is not to be understood in terms of a simple extrapolation of the properties of a few particles."

— P. W. Anderson

Anselmo Marques

Supercondutores de múltiplas bandas frustrados

Frustrated Multiband Superconductors

Dissertação apresentada à Universidade de Aveiro para cumprimento dos requisitos necessários à obtenção do grau de Mestre em Física, realizada sob a orientação científica do Doutor Ricardo Assis Guimarães Dias, Professor Auxiliar do Departamento de Física da Universidade de Aveiro

o júri / the jury

presidente / president

Manuel António dos Santos Barroso
Professor Auxiliar da Universidade de Aveiro

vogais / examiners committee

Ricardo Assis Guimarães Dias
Professor Auxiliar da Universidade de Aveiro (orientador)

Miguel António da Nova Araújo
Professor Auxiliar da Universidade de Évora (arguente)

Acknowledgements

I would like to begin by thanking my advisor, Prof. Ricardo Dias, for his steady guidance and ready availability in helping me overcome the many obstacles that I had to face throughout my academic path in general, and in the making of this dissertation in particular.

I would also like to thank my family: my parents for supporting me over the years and for giving me the freedom and encouragement needed for me to follow studies in Physics, and my brothers, with whom I have had the pleasure of growing up.

Finally, a word of thanks goes to my friends Carlos, Correia, Fábio, Juta, Melo, Prezas and Santiago, as well as to the rest of the Oldschool Gentlemen's Club, for their spirit of camaraderie and for all the days (and nights) whose awesomeness I will not soon forget.

Palavras-Chave

Supercondutividade, compostos baseados em ferro, múltiplas bandas, frustração

Resumo

Motivada pela recente descoberta de supercondutores baseados em ferro, com altas temperaturas críticas e possibilidade de coexistência de múltiplas bandas no nível de Fermi, esta dissertação pretende estudar as condições sob as quais se podem manifestar configurações frustradas nas fases supercondutoras, em função das variáveis temperatura e campo magnético externo aplicado. A acção recíproca entre as interacções atractivas/repulsivas interbandas e intrabandas é analisada, sendo apresentado o diagrama de fases de campo magnético *vs.* temperatura para um regime de acoplamento entre bandas fraco.

Keywords Superconductivity, iron based compounds, multiple bands, frustration

Abstract Motivated by the recent discovery of iron-based superconductors, having high critical temperatures and multiple bands crossing the Fermi level, this dissertation aims to study the conditions under which frustrated configurations in the superconducting phases can be present, as a function of the variables temperature and externally applied magnetic field. The interplay between interband and intraband attractive/repulsive interactions is analysed, with the magnetic field *vs.* temperature phase diagram being presented for the weakly interband coupling regime.

Contents

Contents **i**

List of Figures **iii**

1 Introduction **1**
1.1 Iron based superconductors 2

2 Multiband Ginzburg-Landau theory **7**
2.1 Type 1 and type 2 9
2.2 Intermediate type 1.5 12

3 Multiband BCS theory **17**
3.1 Free energy derivation 20

4 Frustrated phase configurations **29**

5 Magnetic field in quasi-2D superconductors **35**
5.1 Zeeman splitting effect and Fulde-Ferrel state 36
5.2 Two coupled bands in a magnetic field 37
5.3 Induced frustration in a three-band system 39

6 Conclusion **45**

Bibliography **47**

List of Figures

1.1 Crystalline structure of iron-based superconductor families:(a) 1111, (b) 122, (c) 111 and (d) 11. (Reproduced from [8]) 4

1.2 Above: structure of a bilayer of Fe (red) and As (gold) with tetrahedral coordination. Below: Magnetic profile of the iron ions as seen from above. Dashed lines delimit the unit cell. (Reproduced from [9]) 5

1.3 (a) Fermi surface in the first Brillouin zone of a typical iron-based superconductor with a hole pocket at the origin and electron pockets at the corners. Q is the antiferromagnetic nesting vector. (Reproduced from [10]). (b) Fermi surfaces for hole-like (α and β) and electron-like bands (γ and δ) in $Ba_{0.6}K_{0.4}Fe_2As_2$ at 15 k. (Reproduced from [11]). 5

2.1 Magnetization versus parallel applied magnetic field in a cylindrical superconductor for (a) type 1 superconductivity, and (b) type 2 superconductivity. (Reproduced from [13]) 11

2.2 (a) Simulation of the stable configuration of a type 1.5 weakly coupled two-band superconductor for the case of nine flux quanta. **a**- Magnetic flux density, **b** and **c** represent the condensate densities of the type 2 and type 1 bands, respectively. A normal region for the type 1 band in **c** enables the formation of a a vortex cluster in **b**. (b) Same as in (a), but for twenty five flux quanta in the strong coupling regime. Vortices tend to agglomerate in stripes. Axial symmetry is lost and the final configuration strongly depends on the initial conditions considered. (Reproduced from [**babaev**]). 13

2.3 Magnetization as a function of the applied magnetic field for a type 1.5 superconductor. A first-order transition at H_{c1} from a Meissner to a semi-Meissner state with vortex clusters is what mainly distinguishes the magnetization profile of type 1.5 from the type 2 of Figure 2.1-(b). (Reproduced from [**babaev**]) 14

2.4 Vortex configuration for a small applied field in (a) MgB_2, which is a candidate for type 1.5 superconductivity, and (b) $NbSe_2$, a typical type 2 superconducting material. Stripe patterns with a high degree of inhomogeneity in their distribution in (a) clearly contrast with the more or less organized vortex distribution in (b). (Reproduced from [18]) 15

3.1 Normalized gap function for a one-band superconductor. 19
3.2 Normalized functions for (a) entropy, (b) specific heat, (c) internal energy and (d) free energy for a one-band superconductor. A comparison between normal (red) and superconducting (blue) states is shown; $\gamma = \frac{2\pi^2}{3}N(0)k_B^2$ is a constant factor. (a) shows that the presence of superconductivity represents a more ordered configuration of the material relatively to its normal state. A discontinuity at T_c in (b) is consistent with the continuous transition in (d), in accordance with the Ginzburg-Landau theory. 20

4.1 Phase diagram of $\tilde{J}_{31}/\tilde{J}_{23}$ versus $\tilde{J}_{12}/\tilde{J}_{23}$ in the case where one of the interband $\tilde{J}_{ij}$ is negative. Grey areas correspond to the frustrated regions; the boundaries of these regions mark second-order transitions. 32
4.2 (a) Phases and (b) gap functions versus normalized temperature for a superconductor of three weakly coupled bands with one repulsive and two attractive interband couplings. The vertical dotted lines delimit the temperature range in which frustration is present.(c) Path followed (red curve) by this system in the phase diagram. Parameters: $V_{12} = -0.0045$, $V_{22} = 0.95$, $V_{23} = 0.016$, $V_{31} = 0.016$ and $V_{33} = 0.85$, in units of V_{11}. 33
4.3 Same as in Figure 4.2. Parameters: $V_{12} = -1.94$, $V_{22} = 0.94$, $V_{23} = 1.83$, $V_{31} = 1.88$ and $V_{33} = 0.88$, in units of V_{11}. 33

5.1 Orbital and spin pair-breaking effects caused by an applied field (in green). When the field is applied in-plane the orbital effect can be neglected. (Reproduced from [30]) 36
5.2 Field vs. temperature phase diagram for a one-band superconductor. The BD dashed line marks a first-order trasition between normal and superconducting phases; AD and CD lines give the supercooling and superheating fields, respectively; and the line that goes from D to the zero field critical temperature represents a second-order transition. (Reproduced from [3]) . 37
5.3 Lines (a) and (b), and dashed lines (b) and (c) show the up-spin and down-spin fermi surfaces. O is the $k = 0$ point and q is the momentum displacement between surfaces due to Zeeman splitting. (Reproduced from [32]) . . 37
5.4 Field vs. temperature phase diagram for the two-band (a) uncoupled and (b) weakly coupled cases. One-band behaviour is recovered for each band in (a) as expected. For low temperatures two first-order transitions occur in (b) with the first of them, with respect to increasing h, happening inside the superconducting region. (Reproduced from [4]) 38
5.5 Left axis: gap values in the weakly coupled case as a function of the applied field for T=0. Right axis: free energy difference between superconducting and normal phases. The free energy difference reveals the existence of two first-order transitions: one at A, within the superconducting phase, and another at B, where the system turns normal. (Reproduced from [4]) . . . 39

5.6 Field vs. temperature phase diagram for a system of three weakly coupled bands with one of the interband interactions being repulsive. Normalization values are h_{c0}, the critical field for zero temperature, and T_{c0}, the critical temperature for zero field. h_1, h_2, h_c and h_f are, respectively, the first and second first-order transitions, the critical field and the field that marks the crossing from or to frustrated regions, which correspond to the grey area and to the area between dotted grey lines for low temperatures. Shaded red, green and blue areas are regions of metastability for each different first-order phase transition and are limited by the corresponding supercooling field from below and by the superheating field from above. The inset shows the existence of a second frustrated region (dark blue area) within the first one. Vertical dotted lines with red points and letters refer to the three cases shown in Figure 5.7. 42

5.7 Solutions for Δ_1, Δ_2, Δ_3, ϕ_2, ϕ_3 and $\Delta F = F_s - F_n$ for three situations, one in each column: $T = 0.15T_{c0}$, $T = 0.27T_{c0}$ and $T = 0.6T_{c0}$. The Δ's are all normalized by Δ_{10}, the value for Δ_1 at zero field for each case. The free energy difference is normalized by its absolute value for zero field and the field h by the critical field h_c for the corresponding temperature. ϕ_1 is set to zero as mentioned elsewhere. The letters are guides to the eye for the reader to follow the continuous path and also mark some points of interest shown in Figure 5.6; in the case of the phases, only the letters that mark transitions to or from chiral regions are indicated for ϕ_3. The dotted lines in the free energy graphics give the zero value. 43

5.8 Solutions for Δ_1, Δ_2, Δ_3, ϕ_2, ϕ_3 and $\Delta F = F_s - F_n$ for three different systems, all at $T = 0.2T_{c0}$, and whose couplings matrices, as function of V_{11}, are given in the top of each column. The Δ's are all normalized by Δ_{j0}, the value for Δ_j at zero field for each case, with $j = 1$ for the two first columns and $j = 3$ for the last one. The free energy difference is normalized by its absolute value for zero field and the field h by the critical field h_c. ϕ_1 is set to zero as mentioned elsewhere. The letters are guides to the eye for the reader to follow the continuous path; for the phases only the letters that mark transitions to or from chiral regions are indicated for ϕ_3. The dotted lines in the free energy graphics give the zero value. The DE region in the free energy of the left column is differently coloured so as to highlight a small metastable region within the larger one. Both phases are zero everywhere in the right column. 44

Chapter 1

Introduction

In these past few years, the family of superconducting materials grew considerably when several compounds that include iron in their compositions have unexpectedly shown to exhibit superconductivity, with critical temperatures as high as $T_c = 55$ K [1]. Soon a community of researchers started to form around these new superconducting materials due to a number of interesting characteristics: the above mentioned high-T_c, the presence of multiple bands participating in superconductivity, opening the way to probing for an intrinsic Josephson effect, the requirement for a pairing coupling mechanism stronger than that of the phonon mediated coupling of the BCS theory in order to explain such high-T_c's, the unclear role that antiferromagnetic ordering may play in inducing superconductivity, etc. The problem of intrinsic Josephson currents is closely connected to the possibility of having frustrated phase configurations (where phase differences are neither 0 nor π) in multiband systems; such configurations break time reversal symmetry and create interband supercurrents, in the same way that these can appear in experiments with Josephson junctions due to the presence of phase gradients between different superconducting islands. In a recent paper [2] we addressed the formation of phase frustration and displayed the couplings phase diagram for the case of $n = 3$ bands, where frustrated regions are clearly visible. A summary of the results obtained in this paper is the subject of the Chapter 4 of this dissertation.

But what would happen to this three-band system if we turned on an external magnetic field, keeping the temperature constant? Will frustration be present, presumably only in a specific interval of values of field and temperature? It is now a well known result that at low temperatures the transition from the superconducting to the normal state becomes a first-order one [3]; for a coupled two-band system Dias [4] showed the existence of an additional first-order transition within the superconducting state. The main aim of our

work is to extend these results to a three-band case, analysing in particular the possibility of transitions to frustrated phases. So as to take advantage of the quasi-2D structure of these compounds, the field was considered to be applied parallel to the bands, making the Zeeman splitting effect the dominant one.

The remainder of this dissertation is organized in the following way: this introduction is closed with a section containing a topical overview on the structure and characteristics of iron based superconductors. Chapter 2 deals with the Ginzburg-Landau approach to multiband superconductors, distinguishing those of type 1 from those of type 2 and reserving a section to discuss the possibility of a newly proposed mixed type termed 1.5 superconductivity. On Chapter 3 we expose some fundamentals of the microscopic BCS theory extended to multiband superconductors and give the full derivation of the free energy difference between normal and superconducting states in multiband systems, which will be used in concrete examples later on. On Chapter 4 we address the problem of frustrated phase configurations in a three-band system in the absence of any applied magnetic field, stating the necessary conditions for such configurations to be present and providing the interband couplings phase diagram, along with illustrating examples of paths that reflect the temperature evolution of multiband superconductors. Chapter 5 is devoted to the study of superconducting quasi-2D systems under the influence of external in-plane magnetic fields with a section on the Pauli limit of one-band superconductors, a second section on a coupled quasi-2D two-band system under in-plane applied fields where the Zeeman splitting term becomes dominant, and a last section on the numerical results obtained for a frustrated quasi-2D three-band system, focusing in the weakly coupled case but also presenting a comparison with some more strongly coupled systems; the results obtained in this chapter are expected to be particularly relevant for the newly discovered class of iron-based superconductors. Finally, we make some concluding remarks in Chapter 6, summing up and discussing the work and results of the previous chapters.

1.1 Iron based superconductors

In the search for new superconductors it was assumed for a long time by experimentalists that ferromagnetic elements such as iron should be avoided because on a theoretical level singlet electron pairing, characteristic of conventional BCS superconductors, would not be achievable in compounds with these elements. These past few years have proved how wrong this assumption was. Several iron based materials, particularly iron pnictides- compounds

with iron and pnictogens (elements of group 15) in its structure- have been found to be superconducting. The interest of these materials comes from the fact that they are high-T_c superconductors; additionally, many of them are also multiband superconductors which allows for experimental probing of new features like intrinsic Josephson currents, as will be discussed in later chapters. Under optimum doping $La[O_{1-x}F_x]FeAs$ was found in 2007 to achieve $T_c \sim 43$ K under ~ 4 GPa [5], which is even higher than $T_c = 41$ K for magnesium diboride MgB_2. By replacing La with Pr and Ce [6, 7] critical temperatures around $41 - 43$ K interval can be achieved at ambient pressures; in the same year (2008) a chinese group [1] managed to get $T_c = 55$ K with optimally doped $SmFeAsO_{1-\delta}$. Though the term high-T_c was initially used to classify some materials in the cuprate family (materials with copper-oxide layers) with $T_c > 77$ K, the boiling point for nitrogen, it also encompasses now materials, like Fe-based superconductors, that have T_c lower than 77 K but still higher than the theoretical BCS limit of $T_{c,max} \approx 30$ K (where the pairing mechanism is explained by the scattering of electron pairs by the exchange of a virtual lattice phonon). This new class of materials, in turn, requires a model with a stronger pairing mechanism, therefore unconventionally driven superconductivity is expected for iron based superconductors.

Iron based compounds can be divided in four different families:

- $ReOFeAs$ (Re- rare earth) - 1111 family
- $BaFe_2As_2$ - 122 family
- $LiFeAs$ - 111 family
- $FeSe(Te)$ - 11 family

Figure 1.1 shows the crystalline structures of these families while Figure 1.2 depicts the $Fe - As(Se$ or Te in 11 materials) bilayer structure and its spatial spin configuration in the iron strips common to all families.

There are several parameters that allow experimentalists to manipulate the properties of these materials: chemical substitution, doping, pressure, applied fields, charge doping. However, optimization of superconductivity, that is, the way to get the highest possible T_c from a given compound, seems to be universally connected [9] both to a suppression of magnetism and to a tetrahedral bond angle in the bilayer of Figure 1.2 close to the ideal one of $\sim 109,5°$. The close relation that seems to exist between antiferromagnetism and superconductivity in iron-based superconductors has suggested to a large number of researchers that the former may give way to the latter, specifically by pairing processes

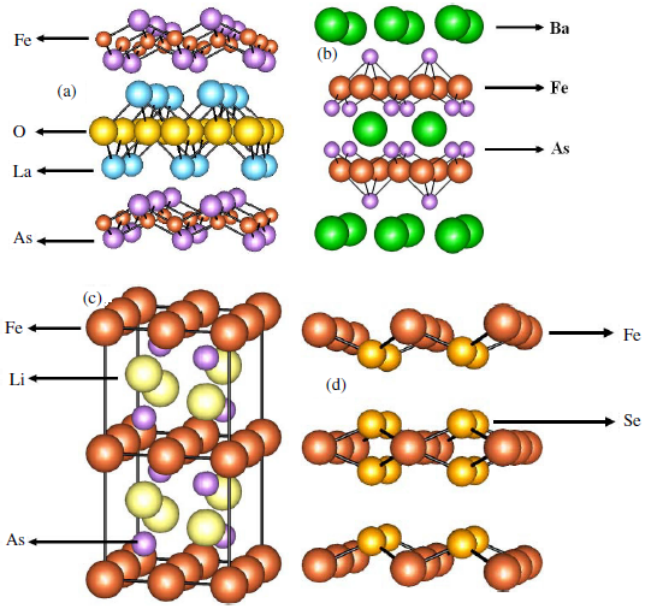

Figure 1.1: Crystalline structure of iron-based superconductor families:(a) 1111, (b) 122, (c) 111 and (d) 11. (Reproduced from [8])

---

involving spin density waves. Scanning the Fermi surface of these materials using techniques like Angle-Resolved PhotoEmission Spectroscopy (ARPES) shows that as a first approximation they can be seen as composed of quasi-2D parallel fermi pockets: the basic feature drawn from the $Fe - As$ structure common to all families is the existence of a hole pocket at the origin (Γ point) and an eletron pocket at the corners (M point) of the first Brillouin Zone as shown in Figure 1.3-(a). Contrary to the cuprate class where the superconducting gap presents an overall d wave gap symmetry, the iron-based compounds display an extended $s\pm$ wave symmetry (a sign reversal in the gap phase between pairs of hole and electron pockets).

The fermiology of more complex structures such as $Ba_{0.6}K_{0.4}Fe_2As_2$ at 15 K [11] can reveal as much as four different fermi surfaces (bands)- two hole-like and two electron-like- each with its own, yet correlated, gap function [see Figure 1.3-(b)]. The slight anisotropy found in the k-dependence of the gap function is consistent with the extended s-wave scenario for each band.

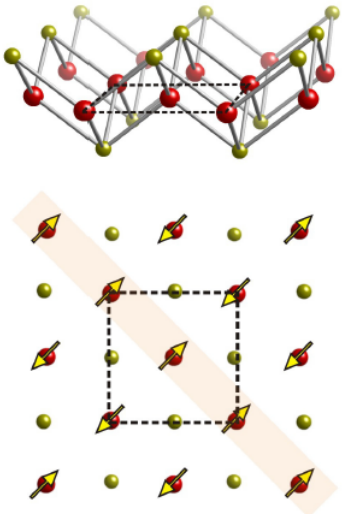

Figure 1.2: Above: structure of a bilayer of Fe (red) and As (gold) with tetrahedral coordination. Below: Magnetic profile of the iron ions as seen from above. Dashed lines delimit the unit cell. (Reproduced from [9])

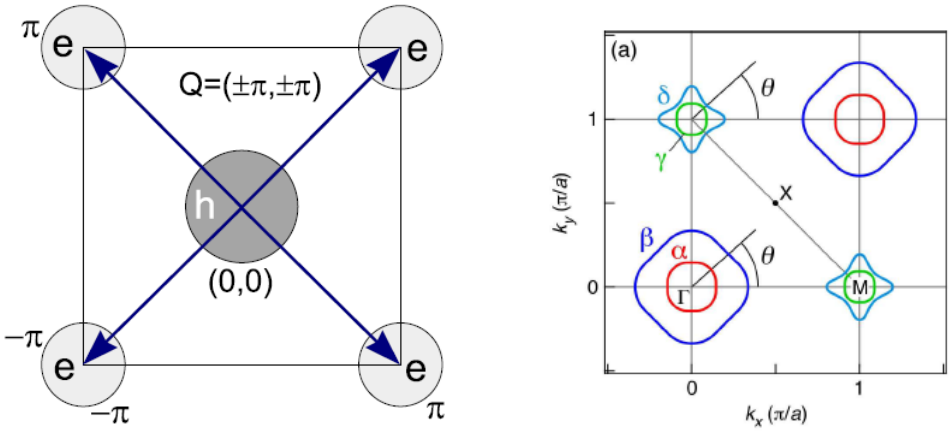

Figure 1.3: (a) Fermi surface in the first Brillouin zone of a typical iron-based superconductor with a hole pocket at the origin and electron pockets at the corners. Q is the antiferromagnetic nesting vector. (Reproduced from [10]). (b) Fermi surfaces for hole-like (α and β) and electron-like bands (γ and δ) in $Ba_{0.6}K_{0.4}Fe_2As_2$ at 15 k. (Reproduced from [11]).

Chapter 2

Multiband Ginzburg-Landau theory

Whenever a physical system undergoes a second-order phase transition, that is, a dissipationless (no latent heat) transition to a lower and spontaneously broken symmetry configuration, Landau theory proves to be very helpful in giving an accurate phenomenological description of the behaviour of the system around the transition point. The simplicity of its basic mechanism bears the mark of ingenious thinking: one starts by expanding the free energy around the transition point in terms of an order parameter (that is zero beyond and non-zero below this point) that models the transition; then one keeps only terms that preserve the symmetry of the system. Minimization of the free energy yields the parameters and equations that describe the transition.

The superconducting transition in the absence of magnetic field is one example of a second-order phase transition (if application of magnetic fields is considered, there will be a temperature region where the transition becomes a first-order one). The phenomenological approach to superconductivity is called the Ginzburg-Landau (GL) theory. Let us apply this theory to our case of interest, consisting of an interacting multiband system. We start by defining the usual order parameter for each band

$$\psi_i(r) = |\psi_i(r)|e^{i\phi_i(r)}, \tag{2.1}$$

where the amplitude $|\psi_i(r)|$ is proportional to the square root of the density of superelectrons and $\phi_i(r)$ is the collective phase factor of band i. We simplify notation by omitting, therefore making it implicit, the spatial dependence of $\psi_i(r) \to \psi_i = |\psi_i|e^{i\phi_i}$. It is conve-

nient to work with the free energy density f taken from the free energy equation

$$F = F_0 + \int f d^3r, \tag{2.2}$$

with F_0 being the normal phase value. The generalized free energy density can be written as [12]

$$\begin{aligned} f &= \sum_i \left\{ \alpha_i |\psi_i|^2 + \frac{1}{2}\beta_i |\psi_i|^4 + \frac{\hbar^2}{4m} |D\psi_i|^2 \right\} + \sum_{\substack{i \\ j>i}} J_{ij} |\psi_i||\psi_j| \cos(\phi_i - \phi_j), && (2.3) \\ D &= \nabla - \frac{i2e}{\hbar c}\mathbf{A}, && (2.4) \\ \alpha_i &= a_i(T - T_c), && (2.5) \\ \beta_i &> 0, && (2.6) \end{aligned}$$

where m and e are the mass and charge of the electron, respectively, $\hbar$ is the Planck's constant divided by 2π, c is the speed of light, ∇ is the usual vector differential operator, α_i, a_i and β_i are the Ginzburg-Landau coefficients to be determined. The third term accounts for spatial inhomogeneities (including variations in the vector potential $\mathbf{A}$), and the last term represents the coupling between different bands and is dependent both on the relative phase differences and on the Josephson coupling J_{ij} which can be either attractive (negative) or repulsive (positive) for a given pair of bands. As one should expect there is no distinction in this last term between interband interactions in the same superconductor and interactions between different superconductors coupled *via* Josephson junctions, since both scenarios are formally equivalent.

Combining the free energy minimization of the simple case of a one dimensional single band superconductor in the absence of magnetic fields [13]

$$0 = \alpha\psi + \beta\psi^3 - \frac{\hbar^2}{4m}\left(\frac{d\psi}{dx}\right)^2, \tag{2.7}$$

with the second GL equation, namely the general current equation

$$j = Re\left\{ \psi^\star \frac{e\hbar}{im} \nabla\psi \right\} - \frac{2e^2}{mc}|\psi|^2 A, \tag{2.8}$$

we can define two parameters that play an important role in defining different kinds of superconductors: the coherence length ξ and the penetration length λ which are, respec-

tively, the decaying distance for the superelectron density with respect to its maximum bulk value and the decaying distance for the magnitude of an applied magnetic field, due to the Meissner effect, measured from the boundary between normal and superconducting states. The λ parameter can also be seen as a consequence of the Anderson-Higgs mechanism, according to which the photons become "massive" inside a superconductor in the presence of a magnetic field, leading to a perfect diamagnetic behaviour in the bulk. Both parameters have the same temperature dependence

$$\xi(T) = \left(\frac{\hbar^2}{4maT_c}\right)^{1/2}\left(1-\frac{T}{T_c}\right)^{-1/2} = \xi_0\left(1-\frac{T}{T_c}\right)^{-1/2}, \tag{2.9}$$

$$\lambda(T) = \left(\frac{mc^2\beta}{8\pi e^2 aT_c}\right)^{1/2}\left(1-\frac{T}{T_c}\right)^{-1/2} = \lambda_0\left(1-\frac{T}{T_c}\right)^{-1/2}, \tag{2.10}$$

so that their ratio becomes a temperature independent constant. Solving (2.7) for the homogeneous case (no spatial derivatives), we arrive at the GL solution for the order parameter

$$\psi = \left(\frac{|\alpha|}{\beta}\right)^{1/2}. \tag{2.11}$$

2.1 Type 1 and type 2

The distinction between different types of superconductivity comes from considerations about domain wall energy, *i.e.*, the surface energy density term that arises in the interface between normal and superconducting regions. For this purpose it is convenient to introduce the GL parameter

$$k = \frac{\lambda}{\xi}. \tag{2.12}$$

Depending on this ratio a material may find either a superconducting or normal configuration to be energetically favourable at the crossing region. The qualitative vision can be summed up as: if the superelectron density grows from the surface to its uniform bulk value quicker than the decay rate of a magnetic field inside the superconductor ($\xi > \lambda$) we have type 1 superconductivity where this crossing region is superconducting; if we have the inverse case ($\xi < \lambda$) then it is preferable to the material to lower its interface energy by developing normal regions throughout the superconductor that enclose and trap magnetic flux, called Abrikosov vortices or simply vortices. Each vortex carries an integer multiple of a quantum of magnetic flux Φ_0 (fractional quantum flux in vortices may arise in multiband

superconductors in the interface between regions with different phase configurations [14, 15, 16]). We point out that this distinction is dependent on the presence of magnetic fields. A more precise and quantitative distinction was provided by Ginzburg and Landau in the following way:

$$\begin{cases} k < \frac{1}{\sqrt{2}} & \rightarrow \quad \text{Type 1 superconductor,} \\ k > \frac{1}{\sqrt{2}} & \rightarrow \quad \text{Type 2 superconductor.} \end{cases} \tag{2.13}$$

An analysis of the behaviour of the magnetization as a function of an applied magnetic field further reveals the differences between type 1 and type 2 superconductors: those of type 1 have a magnetization symmetrical of the field [Figure 2.1-(a)], thus are always in a Meissner phase until the thermodynamic critical field H_c is reached and supercondcutivity ends abruptly (the magnetization reveals a discontinuity at H_c); those of type 2 have two relevant sub-regions within the superconducting region [Figure 2.1-(b)]- starting with no applied field and then increasing it the superconductor behaves as a type 1 (same Meissner phase) until a first critical field H_{c1} is reached, beyond which we enter what is called the mixed state where more and more flux (vortices) is able to penetrate the material therefore increasing the ratio of normal-to-superconducting regions, and the magnetization decreases continuously, becoming zero at the second critical field H_{c2} where all superconducting regions vanish. One intuitive explanation for the value of H_{c1} that marks the transition to the mixed state is that it is given by the minimum area enclosing one flux quantum, that is, an area where the radius corresponds to the field penetration length λ

$$\mu_0 H_{c1} \sim \frac{\Phi_0}{\pi \lambda^2}, \tag{2.14}$$

whereas the exact result [17] is given by

$$\mu_0 H_{c1} = \frac{\Phi_0 \ln k}{4\pi \lambda^2}. \tag{2.15}$$

In the mixed state vortices repel each other and may stabilize in configurations which are either solid lattices or liquid.

To prove the quantised nature of the flux trapped in each vortex we start by rewriting the current equation (2.8) as

$$j = -\frac{1}{\lambda^2 \mu_0}\Big(\frac{\hbar}{4\pi e}\nabla\phi + A\Big), \tag{2.16}$$

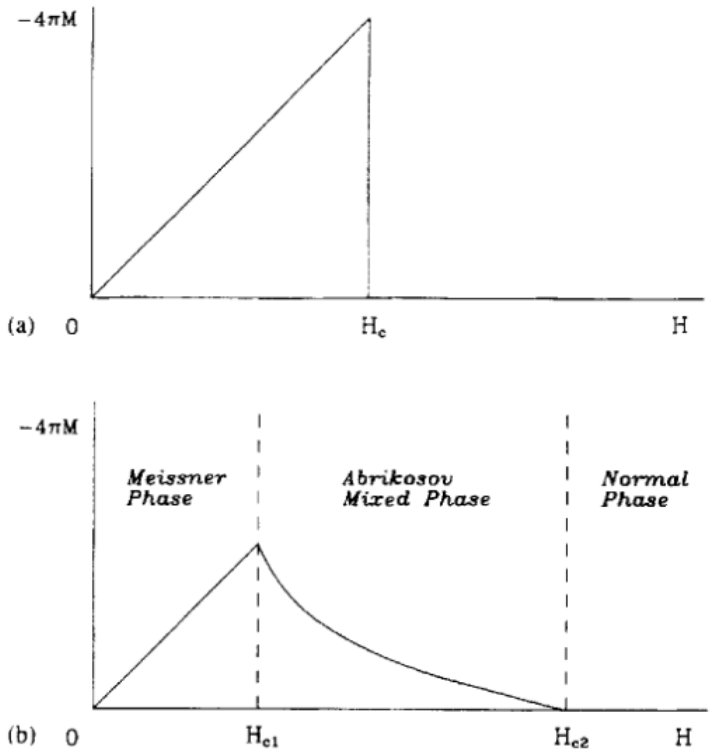

Figure 2.1: Magnetization versus parallel applied magnetic field in a cylindrical superconductor for (a) type 1 superconductivity, and (b) type 2 superconductivity. (Reproduced from [13])

---

where vectorial notation is omitted, μ_0 is the vacuum magnetic permeability and ϕ is the global phase of the order parameter $\psi = |\psi|e^{i\phi}$. Defining a sufficiently large closed loop containing a vortex (with a radius $r \gg \lambda$), so that it encircles a superconducting bulk region where no current flows we can write

$$\oint j dl = -\frac{1}{\lambda^2 \mu_0} \oint \Big(\frac{\hbar}{4\pi e} \nabla\phi + A \Big) dl = 0, \tag{2.17}$$

so that

$$\oint A \; dl = -\frac{\hbar}{4\pi e} \oint \nabla\phi \; dl. \tag{2.18}$$

Using Stokes theorem in the left hand side of (2.18) gives us the flux

$$\oint A \; dl = \iint \nabla \times A \; dS = \iint B \; dS = \Phi, \tag{2.19}$$

whereas the right hand side gives the trivial result

$$\oint \nabla\phi \; dl = 2\pi n, \quad n = 0, \pm 1, \pm 2, ... \quad . \tag{2.20}$$

Inserting back these equations in (2.18) yields

$$\Phi = n\Phi_0, \quad \Phi_0 = \frac{\hbar}{2e}. \tag{2.21}$$

2.2 Intermediate type 1.5

The term 1.5 Superconductivity was first coined in [18] to describe what appears to be some new aspects of the two-band material magnesium diboride MgB_2. This intermediate superconducting type gives rise to a new configuration called semi-Meissner state [19]. As one should expect type 1.5 Superconductivity describes multiband systems where at least one band is type 1 and another type 2. For the case of a two-band superconductor with condensates ψ_1 and ψ_2 and an overall penetration length λ that would mean having

$$\xi_1 < \sqrt{2}\lambda < \xi_2. \tag{2.22}$$

We will follow here mainly the overview article on the subject by E. Babaev *et. al.* [**babaev**]. Since type 1.5 can be thought as partially type 1 and partially type 2, the behaviour of such a system with regard to applied fields must reveal a compromise between opposite tendencies: one to expel all fields up to H_c where the system collapses into a giant vortex (turns normal) in type 1, and another to allow field penetration in the region $H_{c1} < H < H_{c2}$ in the form of quantised vortices that develop encircling currents that shield the superconducting regions from the field, thus making vortex-to-vortex interactions repulsive due to this current-current repulsion. From surface energy considerations it can be shown that in type 1 it is preferable to have one vortex carrying n flux quanta so that the interaction between one flux quantum vortices can be considered attractive because they tend to merge into a single vortex, whereas in type 2 the system prefers to have n flux quanta distributed by n vortices, each carrying Φ_0. Therefore vortex formation in a type 1.5 weakly coupled two-band superconductor is subjected to short-range repulsive interactions due to the type 2 band and to long-range attractive interactions due to the type 1 band, making the system stabilize in a configuration where regions with vortex clusters permeate the superconducting bulk - semi-Meissner state. Each cluster is then composed,

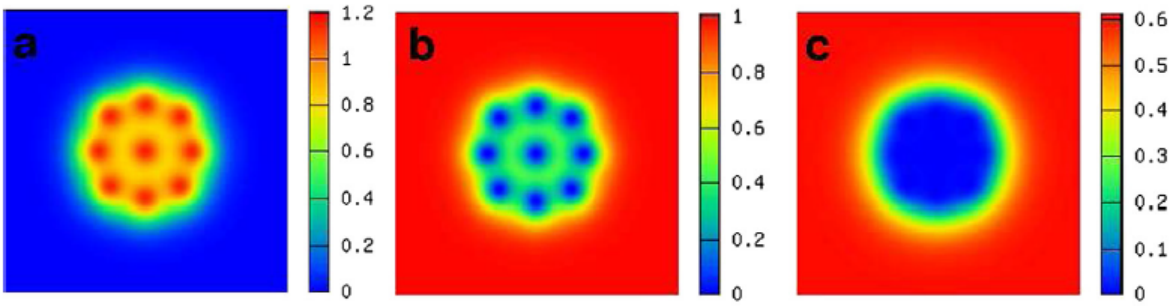

(a)

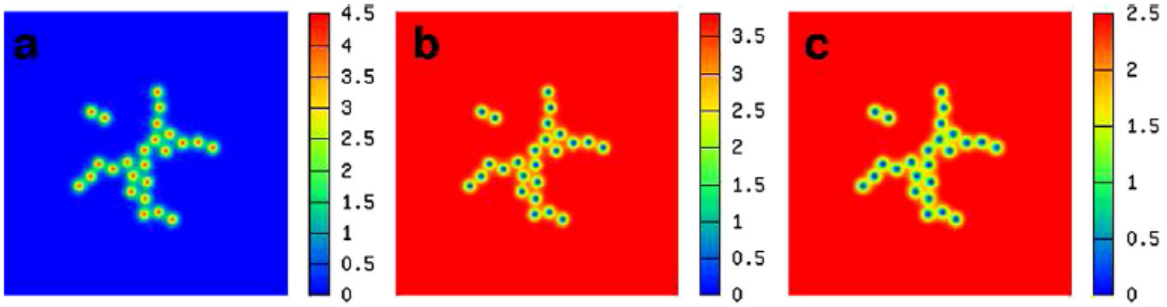

(b)

Figure 2.2: (a) Simulation of the stable configuration of a type 1.5 weakly coupled two-band superconductor for the case of nine flux quanta. **a**- Magnetic flux density, **b** and **c** represent the condensate densities of the type 2 and type 1 bands, respectively. A normal region for the type 1 band in **c** enables the formation of a a vortex cluster in **b**. (b) Same as in (a), but for twenty five flux quanta in the strong coupling regime. Vortices tend to agglomerate in stripes. Axial symmetry is lost and the final configuration strongly depends on the initial conditions considered. (Reproduced from [**babaev**]).

---

qualitatively speaking, of an outer type 1 vortex enclosing several type 2 vortices as shown in Figure 2.2-(a).

However, while this picture may be sufficiently accurate to describe a two-band model in the weakly coupled regime where we have two distinct and almost independent condensates, it fails to explain the regime with stronger couplings where one can no longer speak of independent condensates without incurring in an unjustifiable approximation; in this latter situation we need to find the decoupled normal modes χ_1 and χ_2 of the system which are not directly associated with neither ψ_1 nor ψ_2 but rather represent a rotated version of these fields through a given mixing angle. Instead of a characteristic coherence length defining each band we will now have ξ_1 and ξ_2 associated with the normal modes χ_1 and χ_2. The relation between these new ξ_1 and ξ_2 and λ is what will ultimately determine if a

semi-Meissner state with a magnetization profile like the one in Figure 2.3 can indeed be formed.

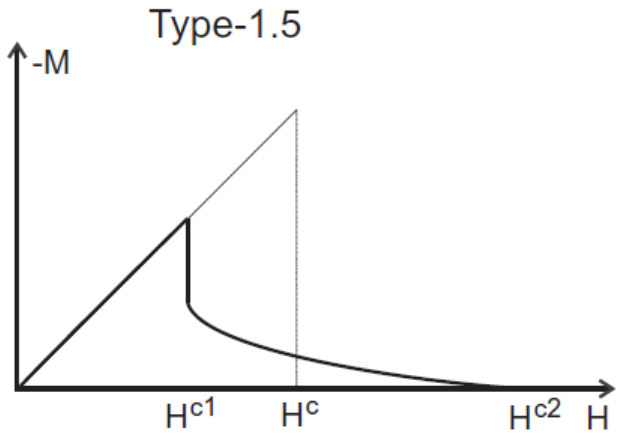

Figure 2.3: Magnetization as a function of the applied magnetic field for a type 1.5 superconductor. A first-order transition at H_{c1} from a Meissner to a semi-Meissner state with vortex clusters is what mainly distinguishes the magnetization profile of type 1.5 from the type 2 of Figure 2.1-(b). (Reproduced from [**babaev**])

The approach followed in [**babaev**] to analyse vortex dynamics was an extended model of that present in [20] that considered vortices as seen for afar, *i.e.*, as interacting point particles with an associated charge q_1 for ξ_1 and q_2 for ξ_2, and magnetic dipole moment m. In terms of field theory this means having q_1, q_2 and m inducing the scalar field masses $\mu_1 \propto \xi_1^{-1}$, $\mu_2 \propto \xi_2^{-1}$ and the vector field mass $\mu_A \propto \lambda^{-1}$, respectively. The interaction energy between point particles has three terms, all of them dependent on their separation distance r

$$E = f_A(\mu_A r) - f_1(\mu_1 r) - f_2(\mu_2 r), \tag{2.23}$$

where the first term corresponds the current-current repulsive interaction and the second and third terms to attractive interactions between point particle pairs of vortices related to the independent fields χ_1 and χ_2. By analysing the behaviour of (2.23) for a given system we can find out if it can develop a semi-Meissner state. For that to happen the vortices must repel each other for small r (E is dominated by the first term) and attract for large r (E is dominated by at least one of the attractive terms). In the example of Figure 2.2-(b) we see a case with strong interband coupling that leads not to an axially symmetric ring-shaped cluster as in the weakly coupled case, but to the formation of a structure with vortex stripes. This appears to be the experimental case observed in MgB_2 [see Figure 2.4-(a)], in contrast with an ordinary Abrikosov vortex lattice of a typical type

2 superconductor [see Figure 2.4-(b)].

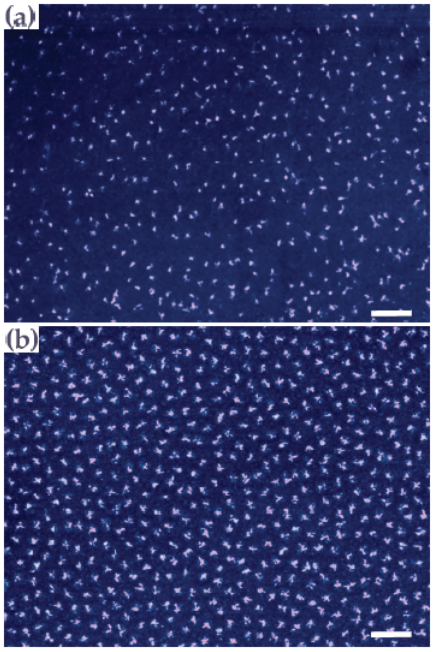

Figure 2.4: Vortex configuration for a small applied field in (a) MgB_2, which is a candidate for type 1.5 superconductivity, and (b) $NbSe_2$, a typical type 2 superconducting material. Stripe patterns with a high degree of inhomogeneity in their distribution in (a) clearly contrast with the more or less organized vortex distribution in (b). (Reproduced from [18])

We stress out at this point that the subject of type 1.5 superconductivity has been an intense field of debate as of lately, with some authors (see, for instance,[21, 22]) disqualifying the possibility of this new state arguing that due to the validity of the GL theory being restricted to a narrow region around the transition temperature, one finds that within this region a single effective coherence length $\xi = \sqrt{\xi_1^2 + \xi_2^2}$ arises in a two-band system, destroying the fundamental requirement for type 1.5 superconductivity, namely, having $\xi_1 < \sqrt{2}\lambda < \xi_2$. In a reply [23] to these articles and in a microscopic treatment of this two-band system [24] by the same authors, it was maintained that hybridization in the two condensates (the normal modes) does translate in the appearance of two distinct coherence lengths and therefore the reduction to a single-component GL model remains unjustified. This in turn lead to a counter-reply [25] where it is sustained that it would be hasty to attribute both the inhomogeneity in Figure 2.4-(a) and the vortex-vortex attractive interaction to a new type of superconductivity, as they may still be explained by type 2 dynamics. Though there is not to date any definitive proof of type 1.5 superconductivity

it can not, however, be categorically ruled out as well. But by the simple fact that this new topic is fomenting serious discussion between supporters of antagonistic claims, some future valuable clarifications about the use of GL models to describe multiband systems may emerge as a product of this debate.

Chapter 3

Multiband BCS theory

It was not until the 1950's, four decades after its discovery by H. K. Onnes, that a theory explaining superconductivity at a microscopic level arose by the hands of Bardeen, Cooper and Schrieffer [26], the original authors of what is now referred to as BCS theory. The underlying idea of it is that superconductivity can be characterized as a microscopic condensation of bound pairs of electrons, called Cooper pairs, into a single quantum state with a collective (global) phase factor. Further considerations show that each Cooper pair is composed of electrons of equal and opposite momentum in a singlet state (spins up and down) so that a Cooper pair can be regarded as a bosonic particle obeying Bose-Einstein statistics. Recently found unconventional superconductors appear to exhibit a ferromagnetically driven formation of Cooper pairs, *i.e.*, spin-triplet states [27, 28]; however a more detailed analysis of this scenario falls outside the scope of this work. For a Cooper pair to form it is necessary that its composing electrons interact in such a way that it is energetically favourable for them to be bounded instead of separated, consequently some form of sufficiently strong attractive potential must be present so as to overpower Coulomb's repulsive potential. The usual picture that illustrates such a potential is that of a lattice phonon mediating the attractive interaction between a pair of electrons: an electron-phonon-electron type of interaction. If thermal agitation in the lattice becomes too strong, it can preclude the occurrence of this process so that low temperatures are required. The condensation energy is given by the difference between superconducting and normal energies

$$E_s - E_n = -\frac{1}{2}N(0)\Delta(T)^2, \tag{3.1}$$

where $N(0)$ is the density of states at the Fermi energy and $\Delta(T)$ is the characteristic superconducting gap energy and can be thought of as the necessary energy to excite a

"quasi-particle"- it will be more clear the meaning of this when we introduce latter on the Bogoliubov transformation; one can see 2Δ as the minimum energy that can break a Cooper pair. Additionally, $\Delta(T)$ can also take the place of the order parameter (see the Ginzburg-Laundau section) in superconductivity since it is only non-zero when this state persists, *i.e.*, until one reaches the transition temperature T_c, called critical temperature, where $E_s = E_n$. Macroscopic condensation into the superconducting state can only occur for electrons in a small strip around the Fermi energy ε_F whose boundaries are given by the Debye frequency ω_D, $[\varepsilon_F - \omega_D \ ; \ \varepsilon_F + \omega_D]$.

In BCS theory it is assumed a ground state in terms of second quantization formalism of the form

$$|\psi_0\rangle = \prod_k (u_k + v_k c^\dagger_{k\uparrow} c^\dagger_{-k\downarrow}) \, |0\rangle \, , \tag{3.2}$$

where $|0\rangle$ is the vacuum state, $|v_k|^2$ gives the probability of occupation for the state $(k \uparrow , -k \downarrow)$ and $|u_k|^2$ the probability that it is unoccupied. Coefficients u_k and v_k can be, in general, complex numbers; with no loss of generality we choose to assign an overall phase to $v_k \to |v_k| e^{i\phi}$, leaving u_k real. We go beyond the classic BCS theory and assume a system of n-bands, each with its own Fermi surface. The ground state is now

$$|\psi_0\rangle = \prod_{j=1}^{n} \prod_k (u_{kj} + |v_{kj}| e^{i\phi_j} c^\dagger_{k\uparrow j} c^\dagger_{-k\downarrow j}) \, |0\rangle \, , \tag{3.3}$$

where the index j runs through all bands present. In this case, we can write the reduced BCS Hamiltonian as

$$H = \sum_{ki} \xi_{ki} c^\dagger_{ki} c_{ki} - \sum_{kk'i} V^{ii}_{kk'} c^\dagger_{k\uparrow i} c^\dagger_{-k\downarrow i} c_{k'\uparrow i} c_{-k'\downarrow i} - \sum_{\substack{kk' \\ i \neq j}} V^{ij}_{kk'} c^\dagger_{k\uparrow i} c^\dagger_{-k\downarrow i} c_{k'\uparrow j} c_{-k'\downarrow j}, \tag{3.4}$$

where $\xi_{ki} = \varepsilon_{ki} - \varepsilon_F$ is the kinetic energy of an electron in the state k of band i measured from the Fermi energy (we assume an absence of magnetic fields at this point and also replaced the chemical potential μ with ε_F since it is a good approximation to assume $\mu(T) \approx cte = \varepsilon_F$), σ is either $\uparrow$ for spin up or $\downarrow$ for spin down, $V^{ii}_{kk'}$ and $V^{ij}_{kk'} = V^{ji}_{kk'}$ are, respectively, the intraband and interband scattering potentials and we further assume the states to be either $(k, \uparrow)$ or $(-k, \downarrow)$. We separated explicitly the second and third terms, concerning the potential part of the Hamiltonian, in order to make clear the important distinction between intraband and interband interactions. Without the interband term we would have an Hamiltonian for a system of non-interacting bands and therefore the relevant

parameters for each band could be extracted from the classic BCS one-band theory. For this one-band system, the gap function is given by

$$\Delta(T) = V \int_0^{\hbar\omega_D} d\xi \frac{N(\xi)}{E} \tanh\left(\frac{E}{2k_B T}\right), \tag{3.5}$$

where the BCS approximations are implied ($\Delta_k, V_{kk'} \to \Delta, V$ in s-wave superconductors), $E = \sqrt{\xi^2 + \Delta^2}$ and k_B is the Boltzmann constant. From the limiting cases $T = 0$ and $\Delta = 0$ we can find expressions both for $\Delta(0)$ and T_c [17],

$$\Delta(0) \simeq 2\hbar\omega_D e^{-1/N(0)V}, \tag{3.6}$$

$$k_B T_c \simeq 1.13\hbar\omega_D e^{-1/N(0)V}, \tag{3.7}$$

where in the phonon frequency region around ε_F we can assume $N(\xi) = N(0)$. Combining both equations gives us the relation between $\Delta(0)$ and T_c predicted by BCS theory

$$\Delta(0) \simeq 1.76 k_B T_c. \tag{3.8}$$

Figure 3.1 shows the universal behaviour of the gap function for a one-band superconductor within the BCS theory, whereas Figure 3.2 displays some relevant thermodynamic quantities of such a system.

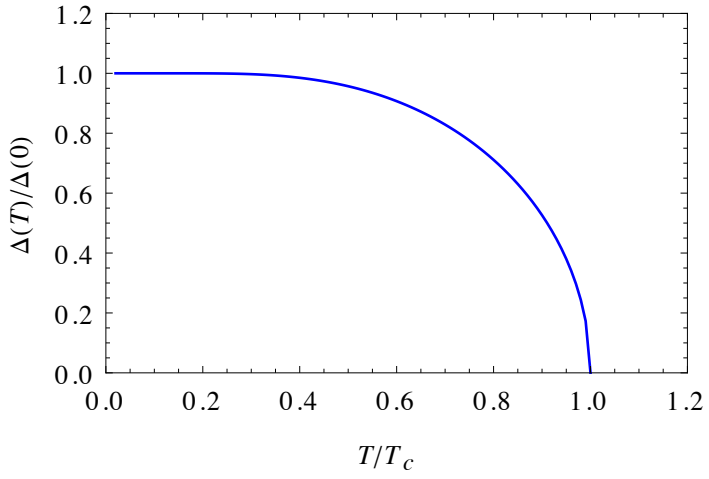

Figure 3.1: Normalized gap function for a one-band superconductor.

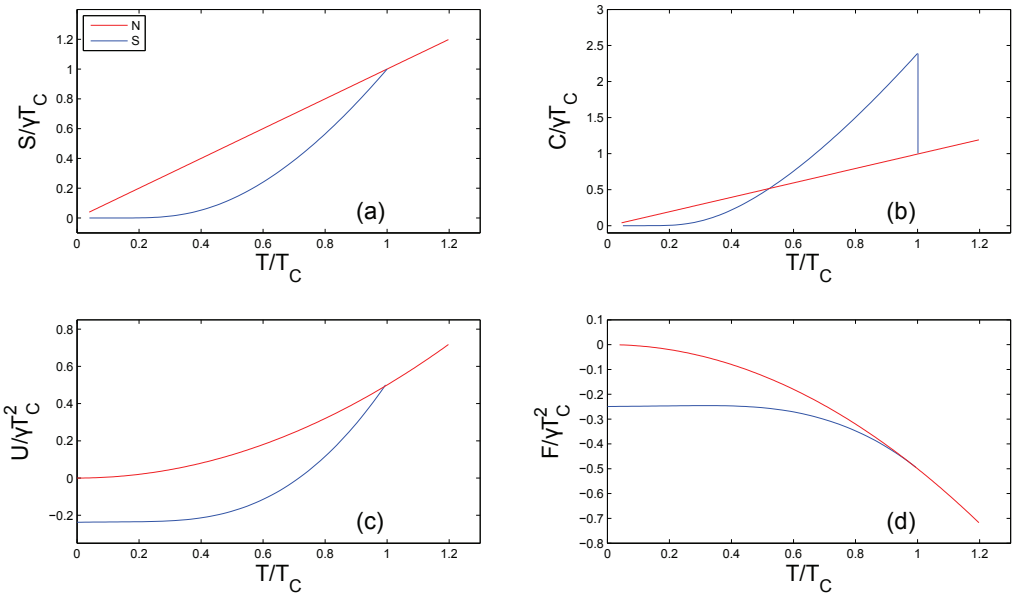

Figure 3.2: Normalized functions for (a) entropy, (b) specific heat, (c) internal energy and (d) free energy for a one-band superconductor. A comparison between normal (red) and superconducting (blue) states is shown; $\gamma = \frac{2\pi^2}{3}N(0)k_B^2$ is a constant factor. (a) shows that the presence of superconductivity represents a more ordered configuration of the material relatively to its normal state. A discontinuity at T_c in (b) is consistent with the continuous transition in (d), in accordance with the Ginzburg-Landau theory.

3.1 Free energy derivation

We will give here the full derivation of the free energy difference between superconducting and normal states for the case we will study later on: that of a multiband quasi-2D superconducting system with in-plane applied magnetic fields. Our reasons to provide the reader with this derivation are twofold:

- In doing so we touch most of the key concepts and reasoning behind BCS formalism.
- Some approximations, e.g. keeping only the Zeeman term as the effect of an applied field, are only relevant and justified in the systems studied in later chapters.

We start by adding a Zeeman term to the Hamiltonian of (3.4)

$$H = \sum_{kj} \xi_{kj}(c^\dagger_{k\uparrow j}c_{k\uparrow j} + c^\dagger_{-k\downarrow j}c_{-k\downarrow j}) - \sum_{kk'ij} V^{ij}_{kk'}c^\dagger_{k\uparrow i}c^\dagger_{-k\downarrow i}c_{k'\uparrow j}c_{-k'\downarrow j} - h\sum_{kj}(c^\dagger_{k\uparrow j}c_{k\uparrow j} - c^\dagger_{-k\downarrow j}c_{-k\downarrow j}), \tag{3.9}$$

where $h = \mu_B H$ is the reduced field, μ_B is the Bohr magneton and H is the strength of the applied magnetic field (that we assume to be in the same direction as the spins). To diagonalize this Hamiltonian we perform a canonical transformation to each band that preserves the fermionic anticommutation rules given by the Bogoliubov-Valatin operators,

$$\begin{pmatrix} c^\dagger_{k\uparrow j} \\ c_{-k\downarrow j} \end{pmatrix} = \begin{pmatrix} u_{kj} & v^\star_{kj} \\ -v_{kj} & u_{kj} \end{pmatrix} \begin{pmatrix} \gamma^\dagger_{k\uparrow j} \\ \gamma_{-k\downarrow j} \end{pmatrix} \longrightarrow \begin{pmatrix} \gamma^\dagger_{k\uparrow j} \\ \gamma_{-k\downarrow j} \end{pmatrix} = \begin{pmatrix} u_{kj} & -v^\star_{kj} \\ v_{kj} & u_{kj} \end{pmatrix} \begin{pmatrix} c^\dagger_{k\uparrow j} \\ c_{-k\downarrow j} \end{pmatrix}, \tag{3.10}$$

$$\left\{ \gamma^\dagger_{k\uparrow i}, \gamma_{k'\uparrow j} \right\} = \delta_{kk'}\delta_{ij}, \tag{3.11}$$

which can be seen as a rotation over the particle creation and annihilation operators plane

$$A = \begin{pmatrix} u_{kj} & -v^\star_{kj} \\ v_{kj} & u_{kj} \end{pmatrix} \longrightarrow \begin{pmatrix} \cos\theta_{kj} & -\sin\theta_{kj} \\ \sin\theta_{kj} & \cos\theta_{kj} \end{pmatrix}, \tag{3.12}$$

by an angle $\theta_{kj} = \arctan\left(\frac{v_{kj}}{u_{kj}}\right)$. Changing the signs of the sines in A gives the transformation relative to the operators $\gamma^\dagger_{-k\downarrow j}$ and $\gamma_{k\uparrow j}$. For instance, $\gamma^\dagger_{k\uparrow j}$ implies adding/removing an electron/hole in the state $(k,\uparrow)/(-k,\downarrow)$ to the renormalized BCS ground state.

Since we are attempting a microscopic description in terms of elementary quasi-particle excitations of a macroscopic system strongly dependent on temperature it is convenient to search for a way to write the Hamiltonian as

$$H = H_0 + c, \tag{3.13}$$

where H_0 is a diagonalized term for non-interacting quasi-particles and c is a constant term representing the thermal average over the entire ensemble. This approach can be found on Rickayzen's book [29]. With the partition function

$$Z = Tr\ (e^{-\beta H}), \qquad \beta = (k_B T)^{-1}, \tag{3.14}$$

it is possible to take the thermal average of an arbitrary operator X (hat notation is implied whenever we speak of operators) as

$$\langle X \rangle = \frac{1}{Z} Tr\ (X e^{-\beta H}). \tag{3.15}$$

With all of this in mind let us decompose the Hamiltonian into a kinetic term K, an interaction term I and a Zeeman term Z,

$$K = \sum_{kj} \xi_{kj} (c^{\dagger}_{k\uparrow j} c_{k\uparrow j} + c^{\dagger}_{-k\downarrow j} c_{-k\downarrow j}), \tag{3.16}$$

$$I = -\sum_{kk'ij} V^{ij}_{kk'} c^{\dagger}_{k\uparrow i} c^{\dagger}_{-k\downarrow i} c_{k'\uparrow j} c_{-k'\downarrow j}, \tag{3.17}$$

$$Z = -h \sum_{kj} (c^{\dagger}_{k\uparrow j} c_{k\uparrow j} - c^{\dagger}_{-k\downarrow j} c_{-k\downarrow j}). \tag{3.18}$$

Substituting the new operators in K yields

$$\begin{aligned} K &= \sum_{kj} \xi_{kj} \Big[u^2_{kj} \big(\gamma^{\dagger}_{k\uparrow j} \gamma_{k\uparrow j} + \gamma^{\dagger}_{-k\downarrow j} \gamma_{-k\downarrow j}\big) + |v_{kj}|^2 \big(\gamma_{k\uparrow j} \gamma^{\dagger}_{k\uparrow j} + \gamma_{-k\downarrow j} \gamma^{\dagger}_{-k\downarrow j}\big) \\ &+ u_{kj} v_{kj} \big(\gamma^{\dagger}_{k\uparrow j} \gamma^{\dagger}_{-k\downarrow j} - \gamma^{\dagger}_{-k\downarrow j} \gamma^{\dagger}_{k\uparrow j}\big) + u_{kj} v^{\star}_{kj} \big(\gamma_{-k\downarrow j} \gamma_{k\uparrow j} - \gamma_{k\uparrow j} \gamma_{-k\downarrow j}\big) \Big]. \end{aligned} \tag{3.19}$$

When averaging this term, non-diagonal terms of the form $\langle\gamma\gamma\rangle$ and $\langle\gamma^{\dagger}\gamma^{\dagger}\rangle$ automatically vanish. The anticommutation rule (3.11) allows us to make use of the identity $\gamma_{k\uparrow j}\gamma^{\dagger}_{k\uparrow j} = 1 - \gamma^{\dagger}_{k\uparrow j}\gamma_{k\uparrow j}$. The average of the fermionic particle operator gives the Fermi distribution function

$$\langle n_{k\sigma j}\rangle = \langle \gamma^{\dagger}_{k\sigma j} \gamma_{k\sigma j}\rangle = f_{k\sigma j} = \frac{1}{1 + e^{\beta E_{k\sigma j}}}, \tag{3.20}$$

where we anticipated the result for the quasi-particle energy spectrum

$$E_{k\sigma j} = \sqrt{\xi^2_k + |\Delta_j|^2} - h\sigma_Z, \tag{3.21}$$

with $\Delta_j = |\Delta_j| e^{i\phi_j}$ being the gap value of band j and σ_z the Pauli matrix in the z direction (the direction of the applied magnetic field) with the correspondence $\sigma = \uparrow, \downarrow \rightarrow \sigma_z = 1, -1$. Since the kinetic energy ξ_k appears in a quadratic form we drop at this point in the γ operators basis the minus sign in the momentum, making the single variable k account for all the possible states. Reminding that $u^2_{kj} + |v_{kj}|^2 = 1$ we are now able to find the thermal average of the kinetic term

$$E_K = \langle K \rangle = \sum_{k\sigma j} \Big[|v_{kj}|^2 \xi_{kj} + \xi_{kj} (u^2_{kj} - |v_{kj}|^2) f_{k\sigma j} \Big]. \tag{3.22}$$

Due to the similarities between the kinetic and Zeeman terms in (3.16) and (3.18) it is easy to combine them to yield

$$E_{KZ} = \langle K + Z \rangle = \sum_{k\sigma j} \left[|v_{kj}|^2 \xi_{kj} + \Big(\xi_{kj}(u_{kj}^2 - |v_{kj}|^2) - h\sigma \Big) f_{k\sigma j} \right]. \tag{3.23}$$

Now only the interaction term is left to average. Just by inspection of I we can see that we only need to average the terms $c^\dagger_{k\uparrow i} c^\dagger_{-k\downarrow i}$ and $c_{k'\uparrow j} c_{-k'\downarrow j}$ since crossed terms with $k \neq k'$ or $i \neq j$ vanish,

$$\begin{aligned} \langle c^\dagger_{k\uparrow i} c^\dagger_{-k\downarrow i} \rangle &= -u_{ki} v^\star_{ki} \langle \gamma^\dagger_{k\uparrow i} \gamma_{k\uparrow i} \rangle + u_{ki} v^\star_{ki} \langle \gamma_{k\downarrow i} \gamma^\dagger_{k\downarrow i} \rangle \\ &= u_{ki} v^\star_{ki} \big(1 - f_{k\uparrow i} - f_{k\downarrow i} \big), \end{aligned} \tag{3.24}$$

$$\begin{aligned} \langle c_{k'\uparrow j} c_{-k'\downarrow j} \rangle &= -u_{k'j} v_{k'j} \langle \gamma^\dagger_{k'\uparrow j} \gamma_{k'\uparrow j} \rangle + u_{k'j} v_{k'j} \langle \gamma_{k'\downarrow j} \gamma^\dagger_{k'\downarrow j} \rangle \\ &= u_{k'j} v_{k'j} \big(1 - f_{k'\uparrow j} - f_{k'\downarrow j} \big). \end{aligned} \tag{3.25}$$

The interaction average can then be written as

$$E_I = -\sum_{kk'ij} V^{ij}_{kk'} u_{ki} v_{ki} u_{k'j} v_{k'j} e^{i(\phi_j - \phi_i)} (1 - f_{k\uparrow i} - f_{k\downarrow i}) \big(1 - f_{k'\uparrow j} - f_{k'\downarrow j} \big), \tag{3.26}$$

where $v_{kj} = |v_{kj}|$ from now on. From the symmetry argument mentioned above that we can interchange two bands with each other ($V^{ij}_{kk'} = V^{ji}_{kk'}$) we rewrite E_I as a sum of an intraband and an interband term

$$\begin{aligned} E_I &= -\sum_{kk'i} V^{ii}_{kk'} u_{ki} v_{ki} u_{k'i} v_{k'i} (1 - f_{k\uparrow i} - f_{k\downarrow i}) \big(1 - f_{k'\uparrow i} - f_{k'\downarrow i} \big) \\ &- 2 \sum_{\substack{kk' \\ j>i}} \cos(\phi_j - \phi_i) V^{ij}_{kk'} u_{ki} v_{ki} u_{k'j} v_{k'j} (1 - f_{k\uparrow i} - f_{k\downarrow i}) \big(1 - f_{k'\uparrow j} - f_{k'\downarrow j} \big). \end{aligned} \tag{3.27}$$

The phase difference factor will prove to be particularly significative when we study later on a three-band model due to the possibility of having frustrated phase configurations as solutions for the free energy minimization.

We are now able to write the Hamiltonian of (3.13) as

$$
\begin{aligned}
H_0 &= \sum_{k\sigma j} E_{k\sigma j}\gamma^{\dagger}_{k\sigma j}\gamma_{k\sigma j}, && (3.28)\\
c &= \sum_{k\sigma j}\left[v^2_{kj}\xi_{kj} + \Big(\xi_{kj}(u^2_{kj}-v^2_{kj}) - h\sigma - E_{k\sigma j}\Big)f_{k\sigma j}\right]\\
&- \sum_{kk'i} V^{ii}_{kk'}u_{ki}v_{ki}u_{k'i}v_{k'i}(1-f_{k\uparrow i}-f_{k\downarrow i})\big(1-f_{k'\uparrow i}-f_{k'\downarrow i}\big)\\
&- 2\sum_{\substack{kk'\\ j>i}}\cos(\phi_j-\phi_i)V^{ij}_{kk'}u_{ki}v_{ki}u_{k'j}v_{k'j}(1-f_{k\uparrow i}-f_{k\downarrow i})\big(1-f_{k'\uparrow j}-f_{k'\downarrow j}\big). && (3.29)
\end{aligned}
$$

The free energy of the superconducting state can be calculated from

$$F_s = -\frac{1}{\beta}\ln Z = -\frac{1}{\beta}\ln e^{-\beta H_0} + c, \tag{3.30}$$

where manipulation of the first term on the right hand side gives

$$-\frac{1}{\beta}\ln e^{-\beta H_0} = -\frac{1}{\beta}\ln\prod_{k\sigma j}\Big(1+e^{-\beta E_{k\sigma j}}\Big) = ... = \frac{1}{\beta}\sum_{k\sigma j}\ln\big[1-f_{k\sigma j}\big], \tag{3.31}$$

and reinserting back in (3.30) yields

$$F_s = \frac{1}{\beta}\sum_{k\sigma j}\ln\big[1-f_{k\sigma j}\big] + c. \tag{3.32}$$

From here we proceed to find some important relations arising from the free energy minimization. To avoid some rather tedious algebraic manipulations we skip some middle steps and present only the relevant solutions. It is convenient, and physically justifiable, to make the following definitions, where we reintroduced a k dependence on the gap function (that also extends to the one hidden in each Fermi distribution function)

$$
\begin{aligned}
\Delta_{ki} &= \sum_{k'}\Bigg[V^{ii}_{kk'}u_{k'i}v_{k'i}\big(1-f_{k'\uparrow i}-f_{k'\downarrow i}\big)\\
&+ \sum_{j\neq i}\cos(\phi_j-\phi_i)V^{ij}_{kk'}u_{k'j}v_{k'j}\big(1-f_{k'\uparrow j}-f_{k'\downarrow j}\big)\Bigg], && (3.33)
\end{aligned}
$$

or in a more condensed fashion

$$\Delta_{ki} = \sum_{k'j} \cos(\phi_j - \phi_i) V^{ij}_{kk'} \delta_{k'j}, \tag{3.34}$$

$$\delta_{k'j} = \sum_{k'} u_{k'j} v_{k'j} \big(1 - f_{k'\uparrow j} - f_{k'\downarrow j}\big). \tag{3.35}$$

We note that by converting this expression into an integral form and assuming $\Delta_{ki} \to \Delta_i$ one has a multiband system of coupled gap functions

$$\Delta_i = \sum_j V_{ij} \cos(\phi_j - \phi_i) \int_0^{\hbar\omega_D} d\xi_j \Delta_j \frac{N_j(\xi)}{2E_j} \left(\tanh \frac{E_j + h}{2k_B T} + \tanh \frac{E_j - h}{2k_B T} \right), \tag{3.36}$$

that reduces to (3.5) in the BCS one-band case. A first equation is extracted from amplitude minimization $\frac{dF}{dv_{ki}} = 0$,

$$2 v_{ki} u_{ki} \xi_{ki} = (u^2_{ki} - v^2_{ki}) \Delta_{ki}. \tag{3.37}$$

Combining it with the normalization condition $u^2_{kj} + v^2_{kj} = 1$ gives

$$v^2_{ki} = \frac{1}{2}\left(1 - \frac{\xi_{ki}}{E_{ki}}\right), \tag{3.38}$$

$$u^2_{ki} = \frac{1}{2}\left(1 + \frac{\xi_{ki}}{E_{ki}}\right), \tag{3.39}$$

$$u_{ki} v_{ki} = \frac{1}{2E_{ki}} \sqrt{E^2_{ki} - \xi^2_{ki}} = \frac{\Delta_{ki}}{2E_{ki}}, \tag{3.40}$$

where $E_{ki} = \sqrt{\xi^2_{ki} + \Delta^2_{ki}}$. Substituting (3.40) back in (3.37) yields

$$u^2_{ki} - v^2_{ki} = \frac{\xi_{ki}}{E_{ki}}. \tag{3.41}$$

From the definition of δ_{ki} we can extract one last relation needed to get the final form of the free energy,

$$\begin{aligned} \delta_{ki} &= \sum_{ki} u_{ki} v_{ki} \big(1 - f_{k\uparrow i} - f_{k\downarrow i}\big) \\ \iff \delta_{ki} &= \sum_{ki} \frac{\Delta_{ki}}{2E_{ki}} \big(1 - f_{k\uparrow i} - f_{k\downarrow i}\big) \\ \iff \delta_{ki} - \sum_{ki} \frac{\Delta_{ki}}{2E_{ki}} &= -\sum_{ki} \frac{\Delta_{ki}}{2E_{ki}} \big(f_{k\uparrow i} + f_{k\downarrow i}\big). \end{aligned} \tag{3.42}$$

Using (3.37 - 3.41) it is possible to simplify the expression for F_s in (3.32) to become

$$F_s = \frac{1}{\beta}\sum_{k\sigma i}\ln\left[1-f(E_{k\sigma i})\right] + \sum_{ki}\left(\xi_{ki}-E_{ki}\right) + \sum_i \delta_i\Delta_i, \tag{3.43}$$

where $f(E_{k\sigma i}) \equiv f_{k\sigma i}$ and we re-inserted the BCS approximations $\Delta_{ki}, \delta_{ki} \to \Delta_i, \delta_i$. Knowing that, relatively to the superconducting state, the normal state corresponds simply to the absence of a gap (condensation) energy, we get the normal free energy directly from F_s

$$\begin{aligned} F_n &= F_s|_{\Delta_i=0} \\ &= \frac{1}{\beta}\sum_{k\sigma i}\ln\left[1-f(|\xi_{ki}|^\sigma)\right] + \sum_{ki}\left(\xi_{kj}-|\xi_{kj}|\right) \\ &= \frac{1}{\beta}\sum_{k\sigma i}\ln\left[1-f(|\xi_{ki}|^\sigma)\right] + 2\sum_{\substack{k<k_F \\ i}}\xi_{ki}, \end{aligned} \tag{3.44}$$

where $|\xi_{ki}|^\sigma = |\xi_{ki}| - h\sigma_z$ and $k_F = \frac{\varepsilon_F}{\hbar}$ is the Fermi momentum. Subtracting the second term of F_s with the second term in F_n yields

$$\begin{aligned} \sum_{ki}\left(\xi_{ki}-E_{ki}\right) - 2\sum_{\substack{k<k_F \\ i}}\xi_{ki} &= \sum_{\substack{k>k_F \\ i}}\left(\xi_{ki}-E_{ki}\right) + \sum_{\substack{k<k_F \\ i}}\left(\xi_{ki}-E_{ki}\right) - 2\sum_{\substack{k<k_F \\ i}}\xi_{ki} \\ &= \sum_{\substack{k>k_F \\ i}}\left(\xi_{ki}-E_{ki}\right) + \sum_{\substack{k<k_F \\ i}}\left(-\xi_{ki}-E_{ki}\right) \\ &= 2\sum_{\substack{k>k_F \\ i}}\left(\xi_{ki}-E_{ki}\right). \end{aligned} \tag{3.45}$$

This way we arrive at the full expression for the free energy difference between superconducting and normal states

$$\begin{aligned} \Delta F &= F_s - F_n \\ &= \frac{1}{\beta}\sum_{k\sigma i}\ln\left[\frac{1-f(E_{k\sigma i})}{1-f(|\xi_{ki}|^\sigma)}\right] + 2\sum_{\substack{k>k_F \\ i}}\left(\xi_{ki}-E_{ki}\right) + \sum_i \delta_i\Delta_i. \end{aligned} \tag{3.46}$$

In our numerical simulations in Chapter 5 we turned (3.46) into the usual integral version over k space. To this effect the second term can be manipulated to become

$$\sum_{\substack{k>k_F \\ i}} \left(\xi_{ki} - E_{ki}\right) \approx -\sum_i \frac{N_i(0)\Delta_i^2}{2}\left[\frac{1}{2} + \sinh^{-1}\left(\frac{\hbar\omega_D}{\Delta_i}\right)\right], \tag{3.47}$$

where the following approximation has been used

$$\sqrt{1+x^2} \approx x + \frac{1}{2x}, \quad x = \frac{\hbar\omega_D}{\Delta_i} \gg 1, \tag{3.48}$$

and as before $N_i(\xi) \simeq N_i(0)$. δ_i and Δ_i are calculated resorting to (3.36). The free energy difference then becomes

$$\Delta F = \frac{1}{\beta}\sum_{\sigma i} N_i(0)\int_0^{\omega_D} d\xi \ln\left[\frac{1-f(E_{k\sigma i})}{1-f(|\xi_{ki}|^\sigma)}\right] - \sum_i N_i(0)\Delta_i^2\left[\frac{1}{2} + \sinh^{-1}\left(\frac{\hbar\omega_D}{\Delta_i}\right)\right] + \sum_i \delta_i\Delta_i. \tag{3.49}$$

Chapter 4

Frustrated phase configurations

In this chapter we will analyse a superconductor with three different bands, each coupled to the others, in the absence of applied magnetic fields. The results found here can be extrapolated to the equivalent system of three independent superconductors connected *via* Josephson junctions, where the Josephson coupling takes the place of the interband coupling, or even to the recently proposed case of a Josephson junction between an iron-based $s\pm$ two-band superconductor and a one-band superconductor.

The interest of the three band-model, relatively to the two-band model, is that we can now have the system spontaneously developing intrinsic frustrated (chiral) phase configurations where time reversal symmetry is broken and persistent supercurrents arise. We write the expectation value of the mean field approximation of the Hamiltonian of (3.28) and (3.29) [2] for the case of no applied fields as

$$\mathcal{H} \ = \sum_i f_i(|\Psi_i|^2) - \sum_i V_{ii}|\Psi_i|^2 - \sum_{i\neq j} V_{ij}|\Psi_i||\Psi_j|\cos(\phi_j - \phi_i), \tag{4.1}$$

where the first term is the kinetic term, the second term is the intraband interaction and the third term is the interband interaction, with the correspondence

$$\Psi_j = |\Psi_j|e^{-i\phi_j} = \sum_k u_{kj}v_{kj}e^{-i\phi_j}\big(1 - f_{k\uparrow j} - f_{k\downarrow j}\big). \tag{4.2}$$

Looking at (4.1) we see that minimization of the energy with respect to the phases only concerns the interband term, which can assume a somewhat more condensed form, $-\sum_{i\neq j} J_{ij}\cos(\phi_j - \phi_i)$, with $J_{ij} = V_{ij}|\Psi_i||\Psi_j|$ being an effective interband coupling, which is symmetric in the couplings matrix ($J_{ij} = J_{ji}$). Written this way it becomes clear

that a parallelism can be made between the interband term and the Heisenberg Hamiltonian of n all-to-all interacting classical XY spin system, where the spin at the position i, $\vec{S}_i = S_i(\cos\theta_i, \sin\theta_i)$, is characterized by its amplitude S_i and by the angle θ_i it makes in the XY plane

$$\mathcal{H}_H = -\sum_{j>i} \tilde{J}_{ij}\cos(\theta_j - \theta_i), \quad \tilde{J}_{ij} = J^H_{ij} S_i S_j, \tag{4.3}$$

where J^H_{ij} is the coupling constant. By making the appropriate substitutions,

$$\begin{cases} \phi_i \to \theta_i, \\ |\Psi_i| \ \to S_i, \\ J_{ij} \to \tilde{J}_{ij}, \end{cases} \tag{4.4}$$

we can go from one problem to the other and still find the same type of solutions regarding the minimization of the Hamiltonian with respect to the phases/angles. This minimization yields simply

$$\begin{aligned} \frac{\partial \mathcal{H}}{\partial \phi_i} &= 0, \\ \sum_j J_{ij}\sin(\phi_j - \phi_i) &= 0. \end{aligned} \tag{4.5}$$

The non-frustrated solutions are given by

$$\begin{aligned} \sin(\phi_j - \phi_i) &= 0, \\ \phi_i - \phi_i &= 0, \pm\pi. \end{aligned} \tag{4.6}$$

We restricted our study to the case of a system with three bands, but the results here obtained can be generalized to any system with $n > 2$ bands. Let us start by imposing for a matter of simplicity that $\phi_1 = 0$ (with no loss of generality). Even though we are attributing a phase to each band the reader should keep in mind that only phase differences between bands have any physical meaning in BCS theory and not the absolute phases themselves. Then, (4.6) gives us the set of non-frustrated solutions of this system

$$(\phi_1, \phi_2, \phi_3) = (0,0,0) \ \vee \ (0, \pm\pi, \pm\pi) \ \vee \ (0, \pm\pi, 0) \ \vee \ (0, 0, \pm\pi). \tag{4.7}$$

Since by symmetry arguments it is equivalent to have a phase of π or $-\pi$ for ϕ_2 or ϕ_3,

(4.7) can be reduced to the study of the following subset of solutions

$$(\phi_1, \phi_2, \phi_3) = (0,0,0) \ \vee \ (0,\pi,\pi) \ \vee \ (0,\pi,0) \ \vee \ (0,0,\pi). \tag{4.8}$$

In order to obtain frustrated configurations, the condition of having at least three bands is necessary yet not sufficient. Other requirements are:

- Having attractive (positive) intraband interactions, J_{ii}, as one expects for any superconductor.

- Having an odd number of repulsive (negative) interband interactions, J_{ij}. The equivalent condition in the Heisenberg Hamiltonian is having an odd number of antiferromagnetic couplings; if we imagine the case of a system of three spins, all with the same magnitude, and coupled antiferromagnetically we see that not all interactions can be simultaneously minimized, therefore leading to frustration, that is, to a compromise between competing interactions that force the system to stabilize in one of the degenerate solutions for the ground state.

Contrary to the non-frustrated solutions given by (4.6), we have to consider also the magnitude of the couplings in finding the frustrated configurations. In fact, such configurations prove to have a rather elaborate dependence on these couplings,

$$(\phi_1, \phi_2, \phi_3) = \pm \left[0, \cos^{-1}(\alpha^-), -\mathrm{sgn}(\frac{a}{b}) \cos^{-1}(\alpha^+)\right], \tag{4.9}$$

where

$$\alpha^{\pm} = \frac{\pm a^2 \mp b^2 - a^2 b^2}{2ab\gamma^{\pm}}, \tag{4.10}$$

$\gamma^+ = b$, $\gamma^- = a$, $a = J_{12}/J_{23}$ and $b = J_{31}/J_{23}$. These solutions only exist if $|\alpha^{\pm}| \leqslant 1$. The $\tilde{J}_{31}/\tilde{J}_{23}$ versus $\tilde{J}_{12}/\tilde{J}_{23}$ phase diagram when one of the interactions $\tilde{J}_{ij}$ is antiferromagnetic (repulsive) is presented in Figure 4.1. Upon variation of the values of the couplings the system can pass from (to) chiral regions, the grey areas in the figure, to (from) non-chiral ones by second-order transitions which occur at the boundaries that separate distinct regions.

Since the couplings are dependent, through $|\Psi_j|$, on the product of coefficients $u_{kj}v_{kj}$ which, in turn, relates to the gap function given in (3.40), there will be an overall dependence of the couplings on temperature T. By solving numerically the system of coupled gap functions of (3.36) for the temperature range $[0, T_c]$ and by tuning the potential parameters

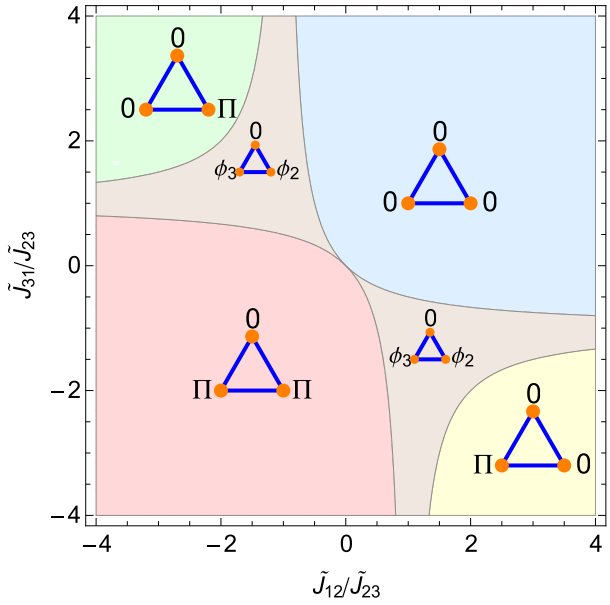

Figure 4.1: Phase diagram of $\tilde{J}_{31}/\tilde{J}_{23}$ versus $\tilde{J}_{12}/\tilde{J}_{23}$ in the case where one of the interband $\tilde{J}_{ij}$ is negative. Grey areas correspond to the frustrated regions; the boundaries of these regions mark second-order transitions.

V_{ij} in our three-band model we can have the system making different paths in the phase diagram with increasing T. Figures 4.2 and 4.3 show, for a system of three bands, the gap functions, the phases as well as their paths in the phase diagram of Figure 4.1 in the cases of weak and strong interband couplings, respectively, with one of them being negative (repulsive) and the other two positive (attractive). The three-band superconductor with weak interband couplings of Figure 4.2 is originally (for $T = 0$) in the non-frustrated region $(0, 0, 0)$, this system then makes a first transition into a frustrated region and a second one again into the non-frustrated region $(0, \pi, 0)$, as shown by the path on the inset. On the other hand, the three-band superconductor with strong interband couplings of Figure 4.3 is originally in a frustrated region and only makes one transition into the same non-frustrated region $(0, \pi, 0)$ in which the system stays until superconductivity is destroyed.

When probing materials for chiral states, with multiband iron-based superconductors being good candidates, experimentalists should test them for various temperature ranges since, as we noted, frustrated configurations might only be possible in a given interval, depending on the specific values for the couplings present in the material.

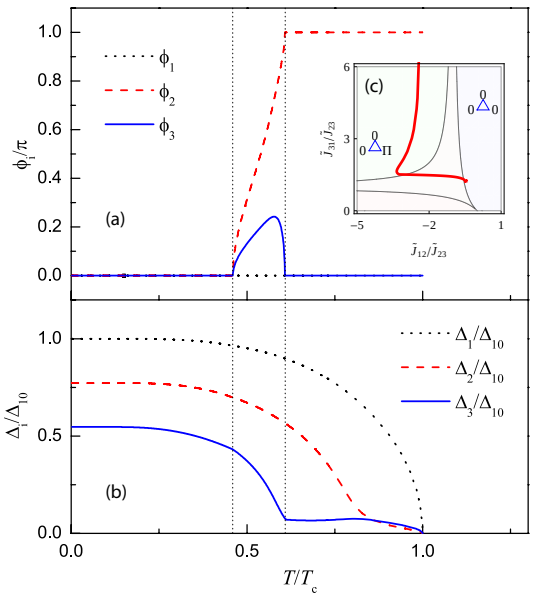

Figure 4.2: (a) Phases and (b) gap functions versus normalized temperature for a superconductor of three weakly coupled bands with one repulsive and two attractive interband couplings. The vertical dotted lines delimit the temperature range in which frustration is present.(c) Path followed (red curve) by this system in the phase diagram. Parameters: $V_{12} = -0.0045$, $V_{22} = 0.95$, $V_{23} = 0.016$, $V_{31} = 0.016$ and $V_{33} = 0.85$, in units of V_{11}.

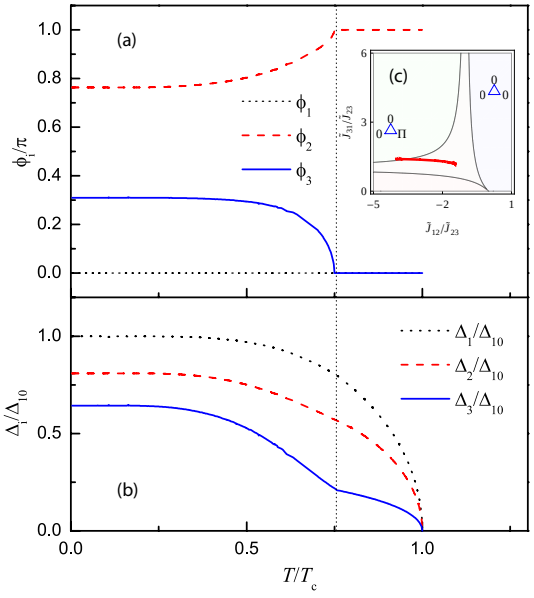

Figure 4.3: Same as in Figure 4.2. Parameters: $V_{12} = -1.94$, $V_{22} = 0.94$, $V_{23} = 1.83$, $V_{31} = 1.88$ and $V_{33} = 0.88$, in units of V_{11}.

Chapter 5

Magnetic field in quasi-2D superconductors

The possibility of having a system making any given path in Figure 4.1 is characteristic of the multiband scenario considered and not of the Heisenberg classical spins model - in it the effective coupling is generally considered to be constant upon variation of temperature, so a system of three spins would have their angles locked in a permanent configuration (a single point in the phase diagram); however, when an external magnetic field is applied, and even though the couplings remains unchanged, the problem is altered with the introduction of extra terms concerning the effect of the field on each individual spin and different paths in the phase diagram may arise if the field is varied. For the case of a multiband superconductor both the interband and the intraband couplings depend on the gap functions which, by (3.36), are temperature and field dependent.

In this chapter we will study the behaviour of a three-band system in the quasi-2D limit, typical of Fe-based superconductors (see chapter 1), under the influence of a varying in-plane external magnetic field h for several fixed temperatures, in order to obtain the h vs. T phase diagram. The fact that the field is applied in-plane simplifies the problem since, as can be seen in Figure 5.1, the effect of orbital pair-breaking of Cooper pairs can be neglected as a first approximation due to the absence of Lorentz forces, leaving the Zeeman splitting effect as the only pair-breaking factor.

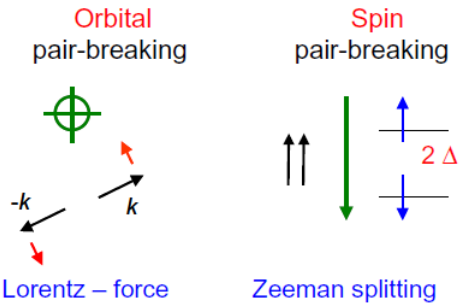

Figure 5.1: Orbital and spin pair-breaking effects caused by an applied field (in green). When the field is applied in-plane the orbital effect can be neglected. (Reproduced from [30])

5.1 Zeeman splitting effect and Fulde-Ferrel state

The response of a one-band superconductor to an applied magnetic field had already been theoretically studied in the 1960's [31, 3]; the phase diagram is shown in Figure 5.2:

- In the line that connects the critical temperature for zero field T_{c0} to D, called the tricritical point $T^\star \approx 0.56 T_{c0}$, the S→N transition is of second-order.
- The BD dashed line marks a first-order transition, where B is the zero temperature critical field called Pauli limit $H_p \simeq \frac{\Delta_0}{\sqrt{2}\mu_B}$.
- The lines AD and CD give the supercooling h_{SC} and superheating h_{SH} fields, respectively, and delimit regions where metastable solutions are present.

In the region BCD a new kind of superconductivity was proposed to be present- the so called Fulde-Ferrel (FF) state, named after the authors of the original paper [31], where the momenta of the electrons in Cooper pairs do not cancel each other but rather display a net momentum $\mathbf{q}$, where $\mathbf{q}$ comes from the displacement between the up-spin and down-spin Fermi surfaces caused by the applied field, as shown in Figure 5.3. If the FF state is indeed present that would mean the first-order transition to be now from the BCS to the FF state, and superconductivity would only be destroyed by a second-order transition at h_{SH}. Another reason to study quasi-2D systems, aside from the fact that orbital effects are neglected, is that there seems to be an enhancement of the FF state due to the low dimensionality that reflects on the optimized nesting condition for pairing, as opposed to 3D spherically symmetric systems; this argumentation was made by H. Shimahara and can be found in [32]. The FF state will not be considered in the remainder of this thesis.

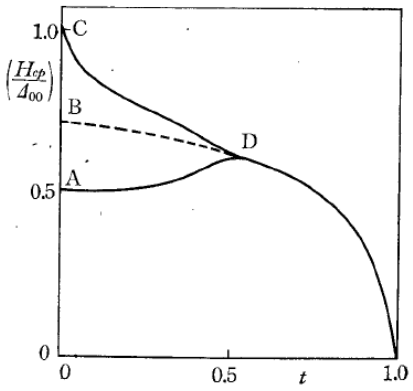

Figure 5.2: Field vs. temperature phase diagram for a one-band superconductor. The BD dashed line marks a first-order trasition between normal and superconducting phases; AD and CD lines give the supercooling and superheating fields, respectively; and the line that goes from D to the zero field critical temperature represents a second-order transition. (Reproduced from [3])

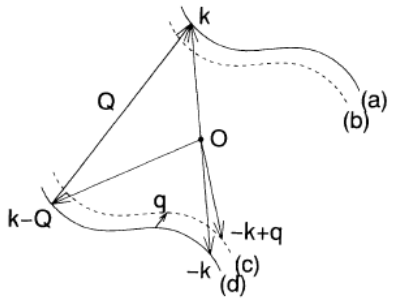

Figure 5.3: Lines (a) and (b), and dashed lines (b) and (c) show the up-spin and down-spin fermi surfaces. O is the $k = 0$ point and q is the momentum displacement between surfaces due to Zeeman splitting. (Reproduced from [32])

5.2 Two coupled bands in a magnetic field

When two bands are present new features emerge if they interact. Obviously for two uncoupled bands one would recover the behaviour of Figure 5.2 for each independent band (see Figure 5.4 (a)). But if we consider the case of two weakly coupled bands we will observe the appearance of an extra first-order transition, but this will happen within the superconducting region (see Figure 5.4 (b)), that is, for low temperatures, the interband coupling prevents the weaker band 2 from becoming normal at the transition point of band 2, keeping it superconducting until the transition of the band 1 occurs. The first-order transition within the superconducting phase is characterized by a large reduction of Δ_2, while little effect is felt by Δ_1. Above the temperature at which the first transition ends

(solid blue line) the phase diagram is dominated by the larger gap Δ_1, becoming similar to the one-band case, even though both bands are still superconducting. Above this region both bands are turned normal at the critical field associated with Δ_1 whether the transition is of first or second order. If we were to increase V_{12} more and more, we would see the metastable yellow region going up, until eventually the first-order transition happening in the superconducting phase would coincide with the S→N transition, consequentially disappearing from thereon.

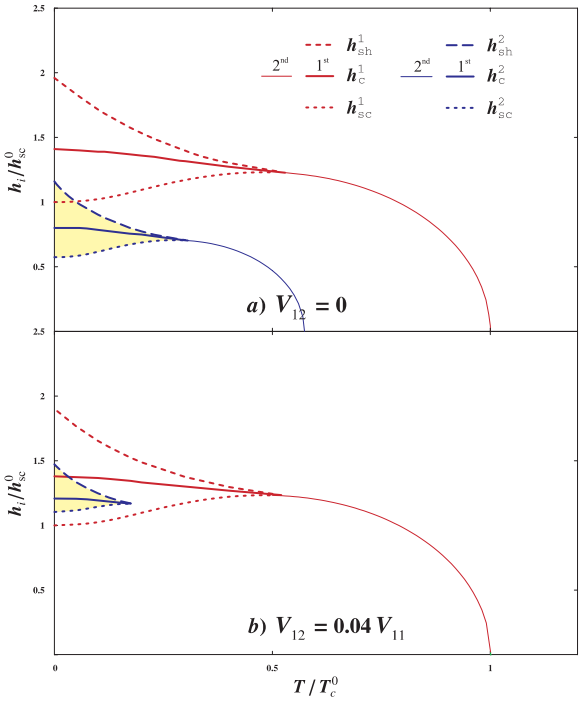

Figure 5.4: Field vs. temperature phase diagram for the two-band (a) uncoupled and (b) weakly coupled cases. One-band behaviour is recovered for each band in (a) as expected. For low temperatures two first-order transitions occur in (b) with the first of them, with respect to increasing h, happening inside the superconducting region. (Reproduced from [4])

An example of the gap functions evolution with field, along with the correspondent normalized values for the free energy difference between superconducting and normal phases, taken for $T = 0$ in the weakly coupled case can be seen in Figure 5.5. We observe in the free energy difference the existence of a first-order transition within the superconducting phase (at point A), where discontinuities in the gap functions occur- a large jump in Δ_2 and a small one in Δ_1, as mentioned before; increasing even further the field value would yield a second first-order transition where the whole system becomes normal (at point B).

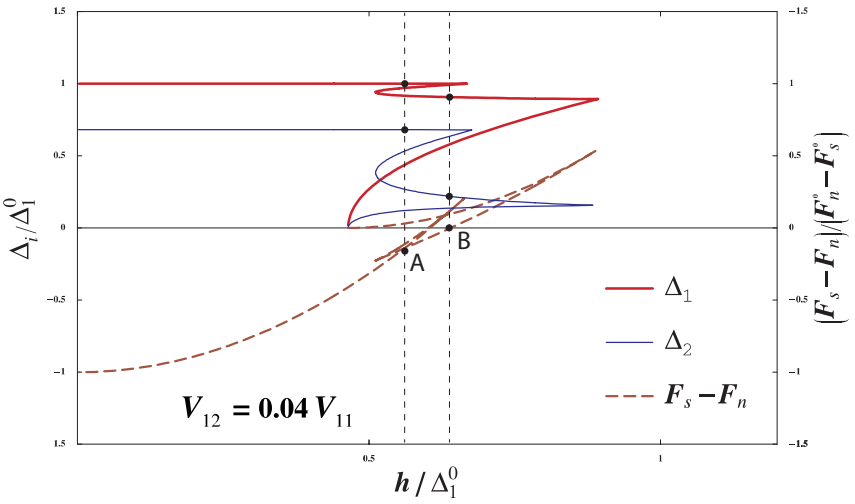

Figure 5.5: Left axis: gap values in the weakly coupled case as a function of the applied field for T=0. Right axis: free energy difference between superconducting and normal phases. The free energy difference reveals the existence of two first-order transitions: one at A, within the superconducting phase, and another at B, where the system turns normal. (Reproduced from [4])

5.3 Induced frustration in a three-band system

For a system of three bands the complexity of the phase diagram is increased due not only to the presence of an extra band, that implies one more first-order transition in the superconducting phase for low temperatures and weak interband couplings, but also to the possibility of having transitions to or from regions of phase frustration if the chosen parameters meet the conditions for such configurations. The case studied here is a system of three weakly coupled bands where one of the interband couplings is repulsive (negative), to ensure the possibility of finding chiral states. The coupling parameters used, in terms of V_{11}, were the following

$$\begin{pmatrix} V_{11} & V_{12} & V_{13} \\ V_{12} & V_{22} & V_{23} \\ V_{13} & V_{23} & V_{33} \end{pmatrix} = V_{11} \begin{pmatrix} 1 & -0.004 & 0.016 \\ -0.004 & 0.95 & 0.016 \\ 0.016 & 0.016 & 0.88 \end{pmatrix}. \tag{5.1}$$

We used a self-consistent method to find the numerical solutions for the bands and their respective phases, from which the free energy difference was calculated using (3.49). The starting assumption for each iteration were the gap values extracted from the system

of coupled gap equations with null phases; then the phases were calculated with these gap values and used to find the new gap values, from which new phases were acquired. The process is then repeated until a convergence criterion is met. The results found this way were condensed into the field versus temperature phase diagram of Figure 5.6. As expected there are now two first-order transitions within the superconducting region for low temperatures. Grey areas show the region where frustrated configurations can be found: for $T \gtrsim 0.37T_{c0}$ the system always crosses this region with increasing field, and there is in fact a specific temperature interval where for zero field the system is already in a frustrated configuration- this possibility was mentioned at the end of the previous chapter. It is interesting to notice that the point where the first transition starts ($T \approx 0.37T_{c0}$) is also the point where the upper and lower limits for frustration are inverted [compare Figure 5.7 (k) and (l)], making the lower limit now coincide with the first supercooling field from here on, meaning that for low temperatures frustrated configurations fall completely in metastable regions. Therefore when the first transition occurs the system jumps from one non-frustrated configuration to another, skipping over the entire region of chirality. Perhaps one sees this more clearly by looking at Figure 5.7 where the behaviour of the system is presented for three different temperatures (the reader is encouraged to cross data with Figure 5.6, with particular emphasis on the correspondence of points marked with letters between figures). Inspection of the phases of the two higher temperature cases reveals the inversion of the frustration limits: if for $T = 0.6T_{c0}$ the system effectively crosses through the frustrated region, the same can not be said about $T = 0.27T_{c0}$ where frustration exists only in the metastable section AB, and since the system skips over this region by a first-order transition (see the free energy difference), there is a discontinuity in ϕ_2, that goes from 0 to π; recalling the couplings phase diagram of Figure 4.1 we expect the path made by the $T = 0.27T_{c0}$ to be the following with increasing field: almost a point in the $(0, 0, 0)$ region and then a discontinuous jump to the $(0, \pi, 0)$ region, followed by two short paths connected by a jump, occurring at the second first-order transition, inside it. For low temperatures, paths in the couplings diagram are limited to non-chiral regions connected by discontinuous jumps at the transition points. For the case where $T = 0.15T_{c0}$ the behaviour of Δ_2 and Δ_3 becomes quite complex, with additional reentrances caused mainly by the appearance of a second smaller frustration region, clearly visible in the phases graphic, and occuring within the region EG in the left column of Figure 5.7. From an experimentalist point of view this region would be of little interest given that it is unlikely that it could be observed in an experiment, regardless of how carefully it is conducted.

Interesting results are found when we invert the premiss of Figure 5.7: we focus now on the behaviour of three different systems, all at the same temperature, chosen to be relatively low ($T = 0.2T_c$, where T_{c0} is the critical temperature of the correspondent system, at zero magnetic field). The cases considered were the following, where the potentials, like in (5.1), are given in terms of V_{11}:

$$(1) \rightarrow \begin{pmatrix} 1 & -0.3 & 0.3 \\ -0.3 & 0.95 & 0.3 \\ 0.3 & 0.3 & 0.88 \end{pmatrix}, \; (2) \rightarrow \begin{pmatrix} 1 & -0.6 & 0.6 \\ -0.6 & 0.95 & 0.6 \\ 0.6 & 0.6 & 0.88 \end{pmatrix}, \; (3) \rightarrow \begin{pmatrix} 1 & -0.5 & 0.8 \\ -0.5 & 0.95 & 0.8 \\ 0.8 & 0.8 & 0.88 \end{pmatrix}. \tag{5.2}$$

The results are shown in Figure 5.8. In case (1) the number of first-order transitions is reduced to two, instead of the three that are present for the same temperature in the weakly coupled case of (5.1); the transition relative to band 2 is still present, somewhere inside the section DE, but falls in a larger region of metastability, appearing after the S→N transition. The system is frustrated from the start and remains that way until the only first-order transition in the superconducting phase is reached, where there is a jump to a non-chiral configuration. By doubling the interband potentials- case (2)- not much is altered, only now there is no DE region as in (1) and the frustrated region is extended a little further. Since for the most part the ratio between the gap functions, and consequentially between the couplings J_{ij} of Chapter 4, is kept almost constant both in (1) and (2), the paths made in the phase diagram of Figure 4.1 are very short in the frustrated region and again in the non-frustrated one, after the transition. Increasing the interband couplings has the effect of shortening the paths made in the phase diagram, by means of reducing the relative change of the gap functions between them. A clear example can be seen in case (3), the right column of Figure 5.8, where the bands are globally more strongly coupled than in (2) (only V_{12} is slightly lower in absolute value), making the respective path amount almost to a single point in the (0,0,0) region. Another effect of increasing the interband couplings, as in the two-band case of the previous section, is to make the first-order transitions within the superconducting phase occur at higher and higher values of magnetic field, to the point where they disappear completely, first only one of them in (1) and (2) and then both in (3), where only the S→N transition is present. It also becomes apparent in (3) the fact that the dominant band is not univocally determined by the biggest intraband potential, since band 3 becomes the dominant one even though $V_{33} < V_{22} < V_{11}$, on account of being more strongly coupled to bands 1 and 2 than these between them ($V_{13} = V_{23} > |V_{12}|$).

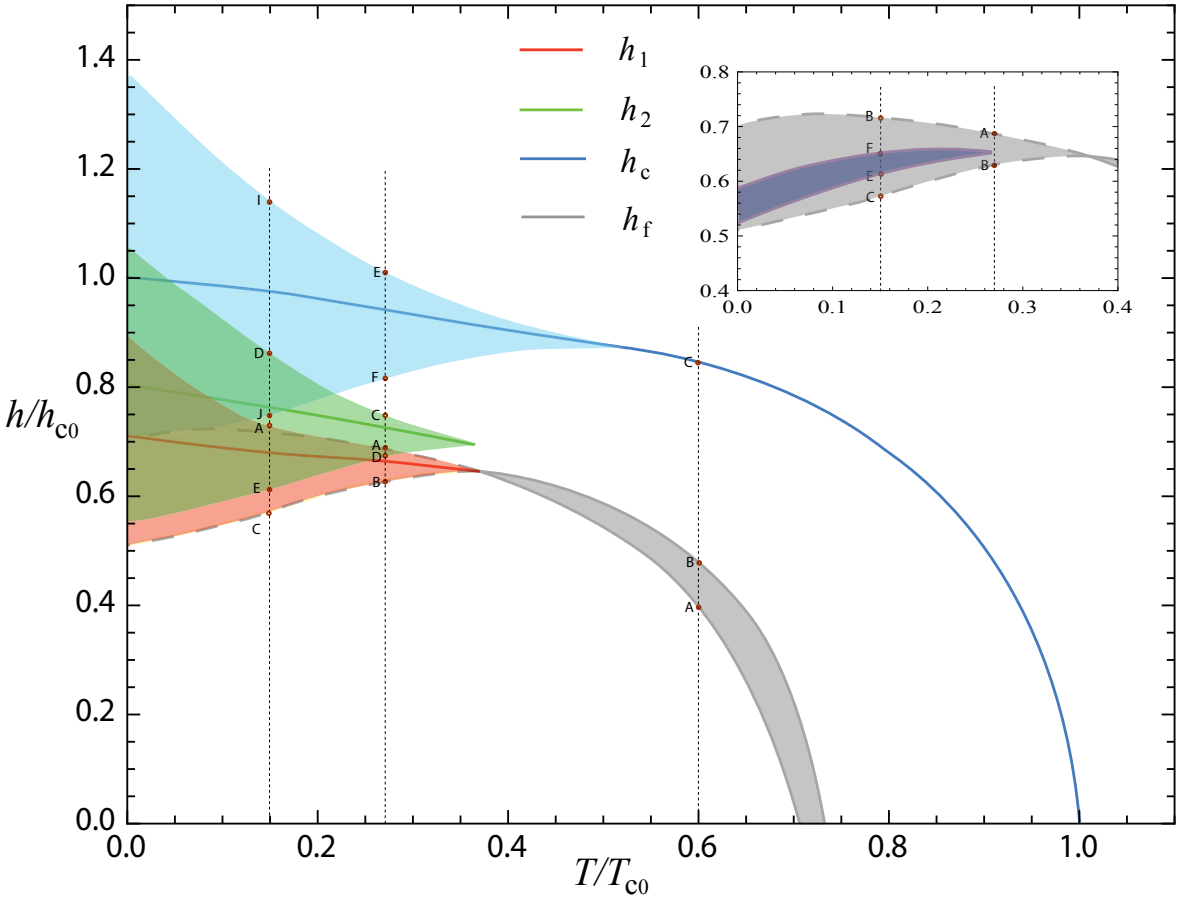

Figure 5.6: Field vs. temperature phase diagram for a system of three weakly coupled bands with one of the interband interactions being repulsive. Normalization values are h_{c0}, the critical field for zero temperature, and T_{c0}, the critical temperature for zero field. h_1, h_2, h_c and h_f are, respectively, the first and second first-order transitions, the critical field and the field that marks the crossing from or to frustrated regions, which correspond to the grey area and to the area between dotted grey lines for low temperatures. Shaded red, green and blue areas are regions of metastability for each different first-order phase transition and are limited by the corresponding supercooling field from below and by the superheating field from above. The inset shows the existence of a second frustrated region (dark blue area) within the first one. Vertical dotted lines with red points and letters refer to the three cases shown in Figure 5.7.

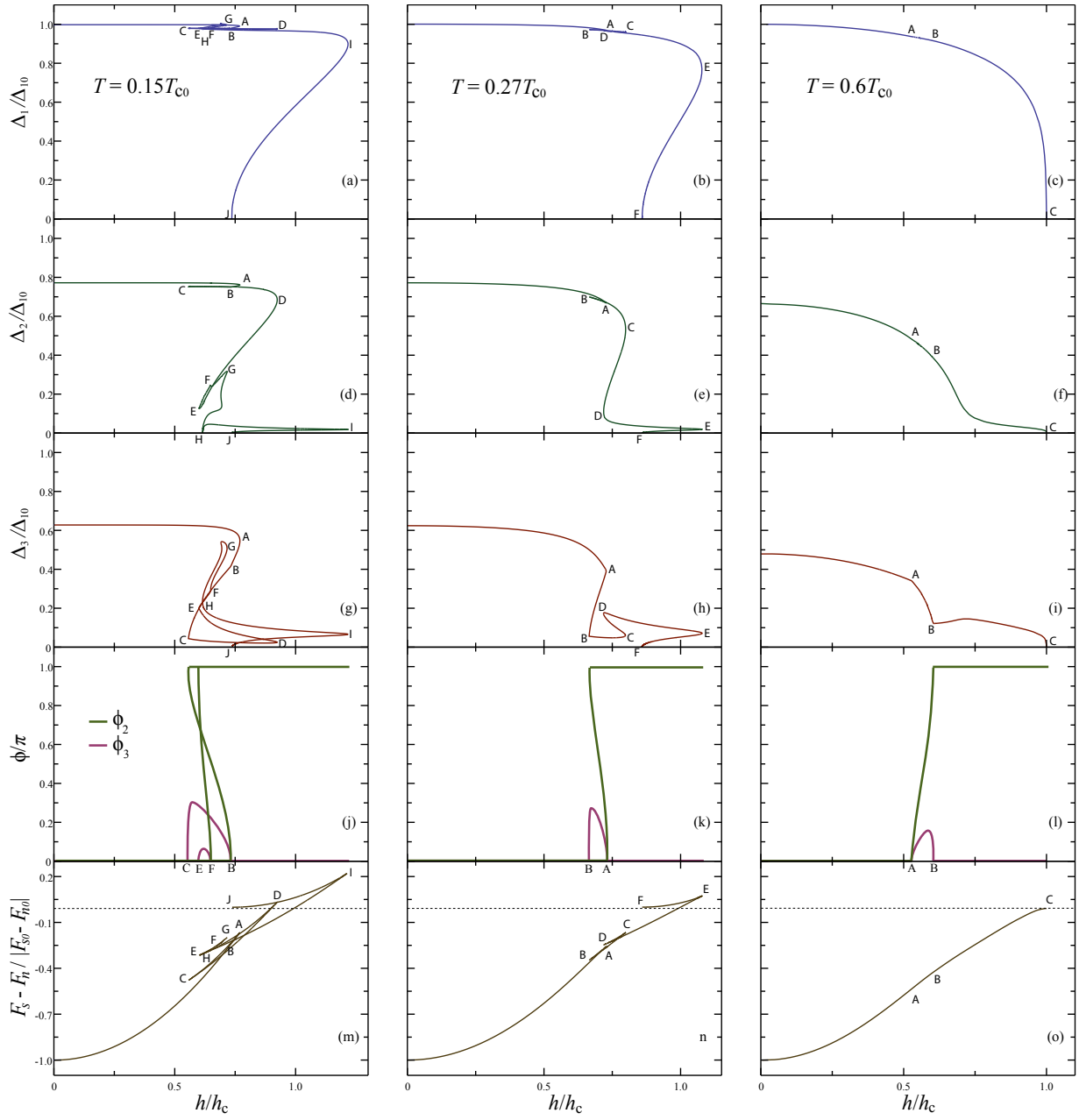

Figure 5.7: Solutions for Δ_1, Δ_2, Δ_3, ϕ_2, ϕ_3 and $\Delta F = F_s - F_n$ for three situations, one in each column: $T = 0.15T_{c0}$, $T = 0.27T_{c0}$ and $T = 0.6T_{c0}$. The Δ's are all normalized by Δ_{10}, the value for Δ_1 at zero field for each case. The free energy difference is normalized by its absolute value for zero field and the field h by the critical field h_c for the corresponding temperature. ϕ_1 is set to zero as mentioned elsewhere. The letters are guides to the eye for the reader to follow the continuous path and also mark some points of interest shown in Figure 5.6; in the case of the phases, only the letters that mark transitions to or from chiral regions are indicated for ϕ_3. The dotted lines in the free energy graphics give the zero value.

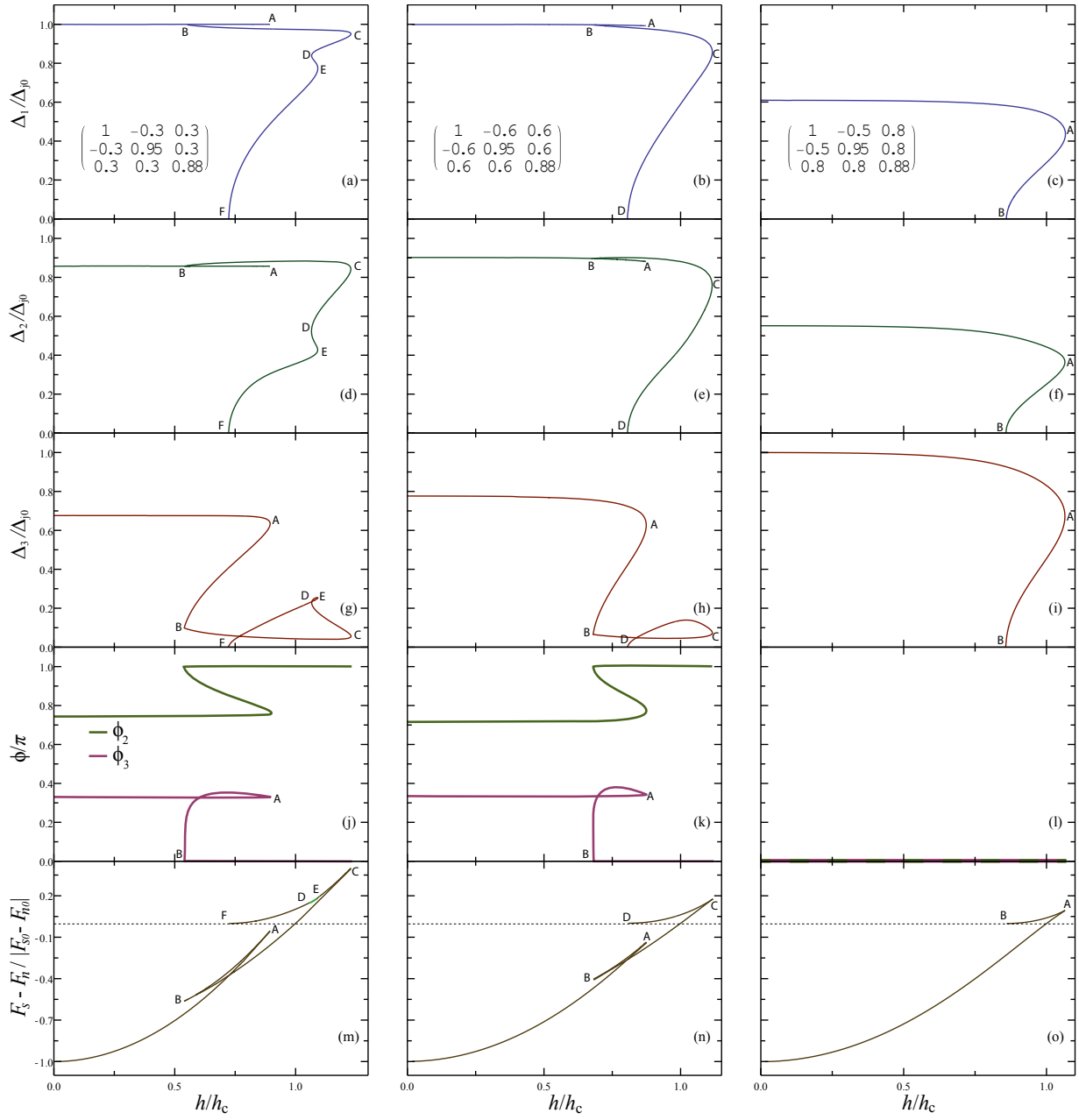

Figure 5.8: Solutions for Δ_1, Δ_2, Δ_3, ϕ_2, ϕ_3 and $\Delta F = F_s - F_n$ for three different systems, all at $T = 0.2T_{c0}$, and whose couplings matrices, as function of V_{11}, are given in the top of each column. The Δ's are all normalized by Δ_{j0}, the value for Δ_j at zero field for each case, with $j = 1$ for the two first columns and $j = 3$ for the last one. The free energy difference is normalized by its absolute value for zero field and the field h by the critical field h_c. ϕ_1 is set to zero as mentioned elsewhere. The letters are guides to the eye for the reader to follow the continuous path; for the phases only the letters that mark transitions to or from chiral regions are indicated for ϕ_3. The dotted lines in the free energy graphics give the zero value. The DE region in the free energy of the left column is differently coloured so as to highlight a small metastable region within the larger one. Both phases are zero everywhere in the right column.

Chapter 6

Conclusion

The discovery of iron-based superconductors has opened a new field for scientific research, full of unanswered questions. The basic *leitmotiv* of this report was to provide the results, and the respective analyses, of some numerical simulations concerning systems that are expected to model the real behaviour of iron compounds. A section of the introduction was reserved to briefly expose the structure and, by means of spectroscopic measurements [11], the Fermi surface of these materials, that attest the validity of the approximations that were made later on, such as: considering the gap functions to be k-independent and the reduced dimensionality of the Fermi pockets correspondent to each band, which can be regarded as quasi-2D [9, 10], subsequently allowing us to retain only the Zeeman splitting term when in-plane magnetic fields are applied.

Superconductivity is a phenomenon whose understanding and description has been historically divided in two complementary approaches: the phenomenological GL theory and the microscopic BCS theory. Feeling that any good theorist working in this field needs to be comfortable in dealing with the basic concepts of both models, we introduced the GL theory extended to multiband systems, giving the distinction between type 1 and type 2 superconductors, important when dealing with vortex dynamics. Some authors [**babaev**, 18, 19] have recently predicted the existence of an intermediate type 1.5 superconductivity based on the vortex distribution of the bilayered compound MgB_2. If in the future it is proven to be true, then new features exhibiting an interplay between type 1 and type 2 opposing tendencies are to be expected. The theoretical background ended with Chapter 3, where we touched some of the key aspects of the generalized BCS theory, pointing out the appearance of factors concerning phase differences in the coupled gap functions that play a crucial role in the systems analysed later on.

If for a two-band superconductor the free energy minimization requires that the phases are either aligned or anti-aligned (the $s\pm$ wave symmetry displayed by some iron-based compounds), the situation changes if one or more bands and an odd number of repulsive interband interactions are present [2]; in this case the stable phase configuration depends on the relative strengths of the couplings involved. In Chapter 4 we showed how three-band systems may lock their phases in values that depart from 0 or π, producing chirality; variation of temperature may cause second-order transitions from or to chiral regions. By tuning the coupling parameters one can manipulate the system to stabilize virtually in any given configuration.

Another way to change the phases configuration is by submitting the system to a magnetic field. By doing so one may see it undergoing one or more first-order transitions, if the temperatures are sufficiently low. In a simple superconductor only the $S \rightarrow N$ transition (or vice-versa) exists. In a multiband system there can be first-order transitions *within* the superconducting phase; this kind of behaviour was only recently predicted in the context of two-band superconductors [4], whereas we extended a similar treatment to the three-band case in Chapter 5, where once again the problem of frustration emerges. It was shown, for weak coupling, that frustrated configurations are only attained in a narrow strip of values for the magnetic field and temperature. A great amount of information can be drawn from the phase diagram of 5.6- perhaps the most striking feature of it being the inversion of the frustration limits coinciding with the beginning of the first first-order transition, meaning that for low temperatures the system skips entirely the frustrated region when the transition happens. For the case of stronger couplings the frustrated strip is expected to be much broader, particularly if the systems start off in a chiral configuration for zero field (cases (1) and (2) of Figure 5.8) and its temperature is low- in such situations the magnetic field seems to have little effect on the phases and gap functions, at least until when one reaches a transition point; this way, frustrated configurations extend to the most part of the $[0, h_c]$ interval, therefore broadening the frustrated strip. On the other side, if the system starts off in a non-chiral configuration, like in case (3), frustration might be completely absent.

An issue that remains open for future work is the extension of our study to short Josephson junction arrays with quasi-2D multiband superconducting elements, addressing once again the magnetic field *vs.* temperature phase diagram. In these systems, the interband tunnellings and the Josephson tunnellings must be considered on an equal footing, leading to a more complex effective symmetry of the arrays.

Bibliography

[1] Zhi-An Ren et al., "Superconductivity and phase diagram in iron-based arsenic-oxides $ReFeAsO_{1-\delta}$ (Re = rare-earth metal) without fluorine doping", *EPL (Europhysics Letters)* 83.1 (2008), p. 17002.

[2] R G Dias and A M Marques, "Frustrated multiband superconductivity", *Superconductor Science and Technology* 24.8 (2011), p. 085009.

[3] Kazumi Maki and Toshihiko Tsuneto, "Pauli Paramagnetism and Superconducting State", *Progress of Theoretical Physics* 31.6 (1964), pp. 945–956, DOI: 10.1143/PTP.31.945.

[4] R. G. Dias, "Zeeman splitting in multiple-band superconductors", *Phys. Rev. B* 72 (1 2005), p. 012505, DOI: 10.1103/PhysRevB.72.012505.

[5] V. G. Stanev, "Multiband Superconductivity in Iron Pnictides and Chalcogenides", PhD thesis, The Johns Hopkins University, 2010.

[6] X. H. Chen et al., "Superconductivity at 43K in $SmFeAsO_{1-x}F_x$", *Nature* 453.7196 (June 2008), pp. 761–762.

[7] G. F. Chen et al., "Superconductivity at 41 K and Its Competition with Spin-Density-Wave Instability in Layered $CeO_{1-x}F_xFeAs$", *Phys. Rev. Lett.* 100 (24 2008), p. 247002, DOI: 10.1103/PhysRevLett.100.247002.

[8] P M Aswathy et al., "An overview on iron based superconductors", *Superconductor Science and Technology* 23.7 (2010), p. 073001.

[9] Johnpierre Paglione and Richard L. Greene, "High-temperature superconductivity in iron-based materials", *Nat Phys* 6.9 (Sept. 2010), pp. 645–658.

[10] D. Parker et al., "Extended $s_{\pm}$ scenario for the nuclear spin-lattice relaxation rate in superconducting pnictides", *Phys. Rev. B* 78 (13 2008), p. 134524, DOI: 10.1103/PhysRevB.78.134524.

[11] K. Nakayama et al., "Superconducting gap symmetry of $Ba_{0.6}K_{0.4}Fe_2As_2$ studied by angle-resolved photoemission spectroscopy", *EPL (Europhysics Letters)* 85.6 (2009), p. 67002.

[12] E. Babaev et al., "Type-1.5 superconductivity in multiband systems: Magnetic response, broken symmetries and microscopic theory A brief overview", *Physica C: Superconductivity* 479.0 (2012), pp. 2 –14, DOI: http://dx.doi.org/10.1016/j.physc.2012.01.002.

[13] J. B. Ketterson and S. N. Song, *Superconductivity*, Cambridge University Press, 1999.

[14] Takashi Yanagisawa et al., "Vortices and Chirality in Multi-Band Superconductors", *Journal of the Physical Society of Japan* 81.2 (2012), p. 024712, DOI: 10.1143/JPSJ.81.024712.

[15] Y. Tanaka et al., "Domains in multiband superconductors", *Physica C: Superconductivity* 471.2122 (2011), pp. 747 –750, DOI: 10.1016/j.physc.2011.05.043.

[16] Julien Garaud, Johan Carlström, and Egor Babaev, "Topological Solitons in Three-Band Superconductors with Broken Time Reversal Symmetry", *Phys. Rev. Lett.* 107 (19 2011), p. 197001, DOI: 10.1103/PhysRevLett.107.197001.

[17] M. Tinkham, *Introduction to Superconductivity*, McGraw-Hill, Inc. , second edition, 1996.

[18] Victor Moshchalkov et al., "Type-1.5 Superconductivity", *Phys. Rev. Lett.* 102 (11 2009), p. 117001, DOI: 10.1103/PhysRevLett.102.117001.

[19] Egor Babaev and Martin Speight, "Semi-Meissner state and neither type-I nor type-II superconductivity in multicomponent superconductors", *Phys. Rev. B* 72 (18 2005), p. 180502, DOI: 10.1103/PhysRevB.72.180502.

[20] J. M. Speight, "Static intervortex forces", *Phys. Rev. D* 55 (6 1997), pp. 3830–3835, DOI: 10.1103/PhysRevD.55.3830.

[21] Jani Geyer et al., "Interface energy of two-band superconductors", *Phys. Rev. B* 82 (10 2010), p. 104521, DOI: 10.1103/PhysRevB.82.104521.

[22] V. G. Kogan and J. Schmalian, "Ginzburg-Landau theory of two-band superconductors: Absence of type-1.5 superconductivity", *Phys. Rev. B* 83 (5 2011), p. 054515, DOI: 10.1103/PhysRevB.83.054515.

[23] Egor Babaev and Mihail Silaev, "Comment on "Ginzburg-Landau theory of two-band superconductors: Absence of type-1.5 superconductivity"", *Phys. Rev. B* 86 (1 2012), p. 016501, DOI: 10.1103/PhysRevB.86.016501.

[24] Mihail Silaev and Egor Babaev, "Microscopic derivation of two-component Ginzburg-Landau model and conditions of its applicability in two-band systems", *Phys. Rev. B* 85 (13 2012), p. 134514, DOI: 10.1103/PhysRevB.85.134514.

[25] V. G. Kogan and Jörg Schmalian, "Reply to "Comment on 'Ginzburg-Landau theory of two-band superconductors: Absence of type-1.5 superconductivity'"", *Phys. Rev. B* 86 (1 2012), p. 016502, DOI: 10.1103/PhysRevB.86.016502.

[26] J. Bardeen, L. N. Cooper, and J. R. Schrieffer, "Theory of Superconductivity", *Phys. Rev.* 108 (5 1957), pp. 1175–1204, DOI: 10.1103/PhysRev.108.1175.

[27] Andriy H. Nevidomskyy, "Coexistence of Ferromagnetism and Superconductivity Close to a Quantum Phase Transition: The Heisenberg- to Ising-type Crossover", *Phys. Rev. Lett.* 94 (9 2005), p. 097003, DOI: 10.1103/PhysRevLett.94.097003.

[28] J. Linder and A. Sudbø, "Quantum transport in noncentrosymmetric superconductors and thermodynamics of ferromagnetic superconductors", *Phys. Rev. B* 76 (5 2007), p. 054511, DOI: 10.1103/PhysRevB.76.054511.

[29] G. Rickayzen, *Theory of superconductivity*, Interscience monographs and texts in physics and astronomy vol. 14, Interscience Publishers, 1965.

[30] G Fuchs et al., "Orbital and spin effects for the upper critical field in As-deficient disordered Fe pnictide superconductors", *New Journal of Physics* 11.7 (2009), p. 075007.

[31] Peter Fulde and Richard A. Ferrell, "Superconductivity in a Strong Spin-Exchange Field", *Phys. Rev.* 135 (3A 1964), A550–A563, DOI: 10.1103/PhysRev.135.A550.

[32] Hiroshi Shimahara, "Fulde-Ferrell state in quasi-two-dimensional superconductors", *Phys. Rev. B* 50 (17 1994), pp. 12760–12765, DOI: 10.1103/PhysRevB.50.12760.